

MSc THESIS

Sensorless control of Permanent Magnet Synchronous Motor at low speed

Subin V Sivasdas

Abstract



CE-MS-2012-04

Motor drives are essential in many industrial applications such as automotive, robotics, power and energy industry. The motor drives need the information of rotor speed to achieve speed control. Rotor speed can be measured by sensors attached to rotor shaft which sends the motor speed to the motor drive. However, using sensors in the rotating shaft is not always practical. A scheme which does not use shaft sensors is required in applications where the working environment is very hostile. This requirement led to the research in the field of sensorless control schemes that estimate the speed of the rotor without any sensors attached to the rotating shaft. The use of machine model helped in estimating the rotor speed by using the phase currents of motor. However, such control schemes still have limitations at low speed because of low signal strength of Back-EMF (Electro Motive Force) in the motor at low speed. Therefore, the sensorless control of motor can not be performed at low speeds. These controlling schemes are useful only above a minimum speed when there is substantial back-EMF in the motor. Hence, applications which require motor control at low speed still rely on shaft sensors to achieve motor control.

The aim of this thesis is to find a method to lower the minimum speed limit of sensorless control close to zero rpm (rounds per minute). Initially a brief study of the existing control schemes was carried out to understand the advantages and disadvantages of each control scheme. Based on this study, current observer sensorless scheme was found to be ideal for developing a sensorless control at low speed. The available current observer scheme does not work for low speeds. Therefore, this scheme was further studied and three improvements were formulated for the scheme. The three improvements suggested are current injection, current averaging and voltage compensation. The current injection and current averaging were then implemented on the current observer scheme. The current injection is done on the direct axis (d-axis) of rotating reference frame. Current injection together with the current averaging are found to reduce the speed limit of existing sensorless control from 450rpm to 50rpm. The stability and power efficiency of the changed control scheme were studied. The algorithm is found to make the control unstable at speed ranges between 220-440rpm. Besides that, the current drawn from the 22V power supply by the motor at speeds less than 200rpm was found to be 1.39A.

Sensorless control of Permanent Magnet Synchronous Motor at low speed

THESIS

submitted in partial fulfillment of the
requirements for the degree of

MASTER OF SCIENCE

in

COMPUTER ENGINEERING

by

Subin V Sivadas
born in Shornur, India

Computer Engineering
Department of Electrical Engineering
Faculty of Electrical Engineering, Mathematics and Computer Science
Delft University of Technology

Sensorless control of Permanent Magnet Synchronous Motor at low speed

by Subin V Sivadas

Abstract

Motor drives are essential in many industrial applications such automotive, robotics, power and energy industry. The motor drives need the information of rotor speed to achieve speed control. Rotor speed can be measured by sensors attached to rotor shaft which sends the motor speed to the motor drive. However, using sensors in the rotating shaft is not always practical. A scheme which does not use shaft sensors is required in applications where the working environment is very hostile. This requirement led to the research in the field of sensorless control schemes that estimate the speed of the rotor without any sensors attached to the rotating shaft. The use of machine model helped in estimating the rotor speed by using the phase currents of motor. However, such control schemes still have limitations at low speed because of low signal strength of Back-EMF (Electro Motive Force) in the motor at low speed. Therefore, the sensorless control of motor can not be performed at low speeds. These controlling schemes are useful only above a minimum speed when there is substantial back-EMF in the motor. Hence, applications which require motor control at low speed still rely on shaft sensors to achieve motor control.

The aim of this thesis is to find a method to lower the minimum speed limit of sensorless control close to zero rpm (rounds per minute). Initially a brief study of the existing control schemes was carried out to understand the advantages and disadvantages of each control scheme. Based on this study, current observer sensorless scheme was found to be ideal for developing a sensorless control at low speed. The available current observer scheme does not work for low speeds. Therefore, this scheme was further studied and three improvements were formulated for the scheme. The three improvements suggested are current injection, current averaging and voltage compensation. The current injection and current averaging were then implemented on the current observer scheme. The current injection is done on the direct axis (d-axis) of rotating reference frame. Current injection together with the current averaging are found to reduce the speed limit of existing sensorless control from 450rpm to 50rpm. The stability and power efficiency of the changed control scheme were studied. The algorithm is found to make the control unstable at speed ranges between 220-440rpm. Besides that, the current drawn from the 22V power supply by the motor at speeds less than 200rpm was found to be 1.39A.

Laboratory : Computer Engineering

Codenumbr : CE-MS-2012-04

Committee Members :

Advisor:

Dr.Ir. Said Hamdioui

Member:

Dr. Jaap Hoekstra

Member:

Dr.Ir. Jos Waegemaekers

Member:

Ing. Sander Straatjes

I dedicate this thesis to my parents and my brother.

Contents

List of Figures	viii
List of Tables	ix
Acknowledgements	xi
1 Introduction	1
1.1 Motivation	1
1.2 Contribution of this thesis	1
1.3 Outline of the thesis	2
2 An overview of PMSM control	3
2.1 Motor Control	3
2.2 PMSM motor	4
2.3 Mathematical Models of motor	5
2.3.1 Motor model on the d-q axis	5
2.3.2 Motor model on the stator reference frame	6
2.4 Conclusions	7
3 Sensorless Algorithms for Motor Control	9
3.1 Classifications	9
3.2 Main sensorless schemes	10
3.2.1 Kalman filter solution	11
3.2.2 Saliency tracking method	11
3.2.3 Fish Method	11
3.2.4 Current observer	12
3.2.5 INFORM method	12
3.2.6 Magnetic Anisotropy	12
3.2.7 Current observer improved	12
3.3 Combination of Solutions	13
3.4 Comparison of the different methods	13
3.5 Conclusions from the survey	14
4 Current Observer Sensorless Scheme	17
4.1 Sensorless FOC with back EMF estimation (current observer)	17
4.1.1 Space vector for three phase circuit systems	17
4.2 Observer Block	22
4.2.1 Slide Mode Controller (+K/-K)	23
4.3 Advantages of FOC	24
4.4 Conclusions	26

5	Improvement in the sensorless scheme	27
5.1	Methods to improve current observer	27
5.2	Current injection	27
5.3	Current Averaging	29
5.4	Voltage Drop Compensation	29
5.5	Integration of improvements into current observer	30
5.6	Conclusion	30
6	Experimental setup and the implementation of proposed schemes	33
6.1	Experimental Setup	33
6.1.1	LPCXpresso motor control board	33
6.1.2	Motor used for testing	34
6.1.3	Software tools	35
6.2	Current injection	38
6.2.1	Steps for the implementation	38
6.2.2	Variation of current injection	39
6.3	Current Averaging Scheme	40
6.3.1	The averaging scheme in signal processing	40
6.3.2	Implementation and results	41
6.4	Conclusions	42
7	Testing of Algorithm	43
7.1	Algorithm testing	43
7.1.1	Angle Estimation testing	43
7.2	Motor Control stability	48
7.3	Power efficiency	48
7.4	Conclusions	49
8	Conclusion and Future Work	51
8.1	Conclusions	51
8.2	Possible improvements in the future	51
	Bibliography	55
A	Appendix	57
A.1	The observer block flow diagram	57
A.2	The Testbench setup	58

List of Figures

2.1	Functional blocks in a motor drive control	3
2.2	The permanent magnet synchronous machine (surface mounted type)	4
2.3	The rotor and stator reference frames	6
2.4	PMSM equivalent circuit in d-q axis	6
2.5	PMSM equivalent circuit of stator side	7
3.1	Comparison of various sensorless control strategies	15
4.1	The space vector representation of two phases in complex plain (real and imaginary axis).	18
4.2	Space vector representation of current vectors in three phases.	19
4.3	Three phase to two phase conversion of vectors	19
4.4	Projection of two phase stationary frame to rotating (d-q) frame.	20
4.5	Basic FOC scheme. Angle theta is obtained from an observer block in a sensorless scheme[8].	21
4.6	Observer block with motor model, slide mode controller, low pass filters(LPF), angle compensation.	22
4.7	Space Vector PWM block	25
5.1	Synchronous frame of PMSM showing the currents causing the flux in the two axes.	28
5.2	Improved Sensorless control block diagram	31
6.1	A brushless DC motor	35
6.2	Motor control software tool.	36
6.3	Software control diagram with input, functions and outputs shown.	37
6.4	Timing diagram.	38
6.5	Testing scheme of Current injection.	39
6.6	Averaging as a low pass filter. The output signal is smooth compared to input.	40
6.7	Low voltage signal with white noise averaged with 4 samples (n=4)	41
7.1	Scope result from GUI comparing the estimated and sensed angle	43
7.2	Angle compensation as a function of speed	44
7.3	The actual rotor speed vs set rotor speed(case 1)	45
7.4	The speed error plotted against the set speed(case 1)	45
7.5	The actual rotor speed vs set rotor speed(case 2)	46
7.6	The speed error plotted against the set speed(case 2)	46
7.7	The actual rotor speed vs set rotor speed(case 3)	47
7.8	The speed error plotted against the set speed(case 3)	47
7.9	The actual rotor speed vs set rotor speed(case 4)	48
7.10	The speed error plotted against the set speed(case 4)	48
7.11	The speed error, +/- 15% of set speed plotted against the set speed	49

A.1	Flow digram of the observer block	57
A.2	Experimental setup	58

List of Tables

5.1	Comparison between the field weakening and current injection	28
6.1	Specification of the motor.[20]	35
6.2	Speed range and averaging size used	42
7.1	Comparison of control performance achieved in different cases	49

Acknowledgements

This thesis would not have been possible without the guidance and support of many people. I wish to thank all of them.

First, I would like to thank my supervisor at Delft, Dr. Said Hamdioui, who gave his support for my thesis. His evaluations and regular Skype discussion with me helped in my progress. I thank him for letting me do a thesis on such a different topic. I would like to thank Jan Bert Kuipers and Sander Strajtees. The discussions we had on the topic of thesis were always insightful and helpful in completing my thesis. I would like to thank Jos Wagaemakers for giving me the necessary support and guidance at NXP. My sincere thanks to all people in the microcontroller group at NXP especially Hassan Naqvi and Herman Moons for providing a good working environment for me to do my thesis.

I would like to thank my friends Vikrant, Vishwa, Shawn, Sudarshan and Bhagath for their encouragement.

Subin V Sivadas
Delft, The Netherlands
October 19, 2012

Introduction

This chapter gives an introduction to the motor control, contribution and the outline of the thesis. In section 1.1 the motivation for the thesis is given. In section 1.2 the contribution of the thesis is enumerated. In the end, section 1.3 gives the organizational outline of the thesis report.

1.1 Motivation

With the increased use of motor drives in many industries such as automobile, robotics, power and energy industry, the study of motor control with digital signal controllers has gained importance in the past couple of decades. The use of microprocessors for controlling the power electronics in a motor drive system has led to a wide range of control mechanism for different kind of motors available.

The earliest intelligent control mechanism for motors involved feedback system in which the values from sensors at the rotation shaft were sent to the digital signal controllers [1]. These sensors gave the position and speed of the motor. Their accuracy and range was limited only by the analog to digital converters (ADC) used in the controllers as well as the physical limitation of the motor itself. However, there are many applications where the hostile working conditions of motor or the cost of sensors makes control schemes with shaft sensors costlier than sensorless control. Thus there were efforts made to achieve the motor control with same accuracy and range of speed without the use of sensors. However, until the last decade the cost of sensorless control was very high because of the lack of cheap high speed controllers. This resulted in very few researches in the field of sensorless control.

With the recent development in the field of microprocessors and digital signal controllers there has been a surge in the study of sensorless solutions which makes use of the new high speed digital signal controllers. There have been many solutions proposed both by researchers in academic institutions as well as by the industries. However it was always a challenge to get the sensorless control at low speed for non-salient motors since at low speed most algorithms either failed or where not accurate enough.[2][3]

1.2 Contribution of this thesis

The objective of the thesis is to develop and implement an algorithm which will improve the sensorless speed control of the PMSM (Permanent Magnet Synchronous Motor) at low speed. The developed algorithm is implemented on NXP's LPC18A50 microcontroller. The contribution and results of the thesis is summarized below.

Contributions:

- (i) The current injection was implemented on a sensorless scheme modeled on rotating reference frame. The injection was done on the direct axis of rotating reference frame with a motive to improve the angle estimation at low speed.
- (ii) The current averaging scheme was implemented on the sensorless scheme along with the current injection to improve the angle estimation at low speed.
- (iii) The effect of current injection and current averaging was analyzed for its stability and power for low speed range (less than 500rpm).

Results:

- (i) The minimum speed that was controlled by sensorless scheme was brought down from 450rpm to 50rpm.
- (ii) Both current injection and averaging was found to improve the speed response at low speed compared to previous sensorless scheme.
- (iii) The instability in the control scheme between 220rpm and 440rpm was identified and studied. The current drawn from the 22V power supply by the motor at speeds less than 200rpm was found to be 1.39A.

The thesis achieved the purpose of having a low speed control of PMSM motor by bringing down the minimum speed at which satisfactory control is achieved. But the power and instability issues of the algorithm has restricted its application in its present form.

1.3 Outline of the thesis

The organization of this thesis is as given below.

Chapter 1 gives the motivation for the thesis and the contribution of the thesis.

Chapter 2 explains the principles behind the modeling and control of Permanent Magnet Synchronous motor.

Chapter 3 presents the classification and comparison of various sensorless control schemes along with the conclusion of the literature survey.

Chapter 4 presents the current observer based sensorless scheme which will be adopted in the thesis in detail along with its limitations.

Chapter 5 gives the proposed improvements to improve the sensorless scheme.

Chapter 6 explains the details of the experiments and test bench. The averaging scheme is presented with its theory and advantages explained. The current injection is presented with the analysis of its effect on the sensorless scheme.

Chapter 7 describes testing of the algorithm and the results of the experiments.

Chapter 8 presents the conclusions of the tests on proposed sensorless schemes along with the scope to improve the scheme in future.

An overview of PMSM control

The purpose of this chapter is to explain the basic motor control used on PMSM and also to give the model of motor used for implementing the controlling schemes. The section 2.1 is about various blocks in the motor control circuit. In section 2.2 the mathematical models of PMSM is explained. Section 2.3 gives the working principle of PMSM and their classification. Finally section 2.4 gives the conclusion of this chapter.

2.1 Motor Control

The basic functional units of an electric motor drive is shown in Fig. 2.1[30]. The functions performed by motor control circuits include starting the motor, protecting the motor from overcurrent, stopping the motor (braking), speed control etc. The motor control scheme used depends on the kind of motor to be controlled and also the application for which it is used.

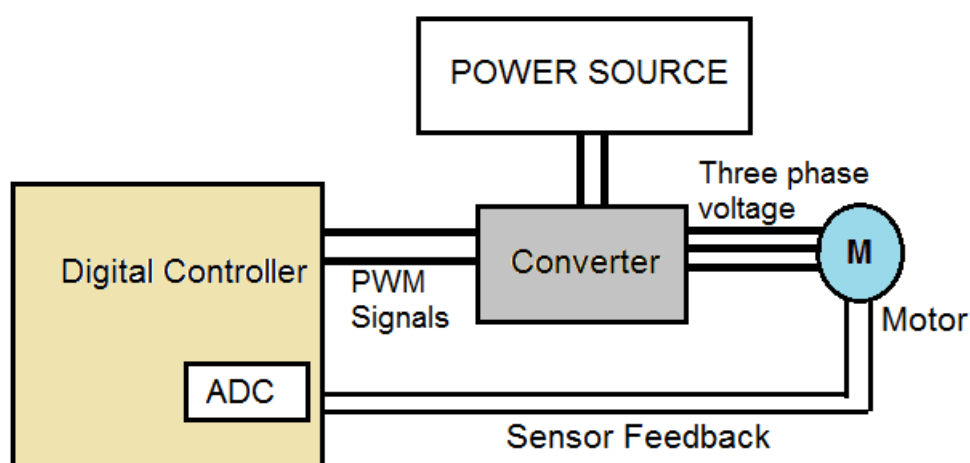


Figure 2.1: Functional blocks in a motor drive control

The speed of the motor is set in the digital controller (Fig. 2.1). The controller generates the PWM (Pulse Width Modulated) signals for the corresponding speed. The converter in the drive system consists of inverters and takes the PWM signals from the controller and converts the DC power to AC power at the required frequency and amplitude. The speed of the motor is sensed using either the shaft sensor or phase currents and fed back to the controller. The controller processes the error in the speed

and adjusts the PWM signals such that the error is minimized. The controller also have provision for detecting overcurrent and give breaking signals accordingly. The PWM signals are generated by a gate driving circuits which is present in the controller itself.

2.2 PMSM motor

A Permanent magnet synchronous motor has characteristics of both induction motor and brushless DC motor. Just like the brushless DC motor, the rotor has a permanent magnet. The stator on the other hand is like induction machine with three phase windings that produces sinusoidal flux in the air gap. Since no current from the stator is used for inducing rotor currents as in induction machine, the power density for a PMSM is higher than induction machine of same size. Because of the robust control which can be achieved using the vector control, the Permanent Magnet Synchronous Motor (PMSM) is favored for sensorless control[12][23][27]. With the use of Digital Signal Controllers (DSC) in vector control, the PMSM type of motors are gaining more popularity. This has led to their use in wide range of applications. The current application of PMSM varies from washing machines to delicate surgical application. Taking this into consideration, this thesis explores the sensorless control of PMSM.

The PMSM is classified into two basic types based on the position of magnet-internal permanent magnet (IPM) and surface permanent magnet (SPM)[17]. In internal permanent type the magnet is buried inside the rotor core, while in the surface permanent magnet the magnet is in the periphery of the rotor. Figure 2.2 shows a surface mounted PMSM motor with a pole pair mounted on the surface of the rotor.

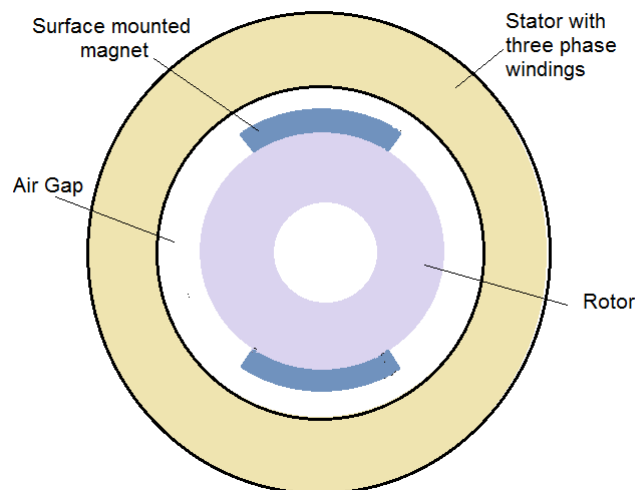


Figure 2.2: The permanent magnet synchronous machine (surface mounted type)

The back EMF(Electro Motive Force) of PMSM is sinusoidal in shape[1]. Therefore,

the three phase stator windings also require sinusoidal current supply. When the three phase windings are energized, the stator also creates a magnetic force. The interaction between this field and the magnetic field of the permanent magnets in the rotor creates a force that rotates the rotor.

2.3 Mathematical Models of motor

The PMSM motor can be modeled on two types of reference frames [15][19]. The stator of PMSM has three phase windings. To represent the voltages in three phase windings, three vectors a,b,c that have 120 degree spatial angle difference are used (Fig. 2.3). Since these vectors represents the voltages in stationary windings, this frame is called stationary reference frame. When the motor is modeled on the stationary reference frame, the voltages/currents represented by the three vectors are controlled. The phase currents are matched with the reference currents of a set speed and the error signals are used to generate the PWM signals. Methods such as hysteresis control and ramp control uses this principle[16].

As seen in Fig. 2.2, the width of air gap between the rotor and stator is less along the axis of magnet compared to the air gap in the direction perpendicular to axis of magnet. Due to this, the air gap reluctance is varying as the rotor rotates. Therefore, the rotor experiences different magnetic fields when it is along the pole pair and when it is perpendicular to a pole pair. Since the inductance varies with the rotor angle, a 2 phase 'd-q'(direct - quadrature) axis (Fig. 2.3) perpendicular to each other is used to model the rotor [23]. Since the orientation of the 'd-q' axis changes as the rotor rotates, this reference frame is called rotating reference frame or synchronous reference frame.

For modeling the motor on rotating reference frame, the machine equations of PMSM is transformed from the three phase 'a-b-c' frame to the 2 phase 'd-q' frame. The transformation used for this purpose is called "Park Transformation"[23]. This is done to change the sinusoidal phase inductance in the stationary frame to a constant in the 'd-q' frame. Both q and d axis components are separately controlled with PI (Proportional-Integrator) controller to achieve torque and speed control.

2.3.1 Motor model on the d-q axis

Modeling the motor on 'd-q' axis requires two sets of equivalent circuits which represent the parameters in two axis one along the d axis and the other along the q axis (Fig. 2.3)[5]. While writing these equations the inductance value used for the d axis is L_d and the inductance value used for q-axis is L_q . The difference in L_d and L_q depends on the difference of air gap along the magnet and perpendicular to the magnet. While transforming the values in the 'a-b-c' reference frame to the 'd-q' reference frame, the angle θ or rotor position is required. The different inductances (L_q and L_d), creates two different axial properties in the rotor. This is called saliency feature of motor. However

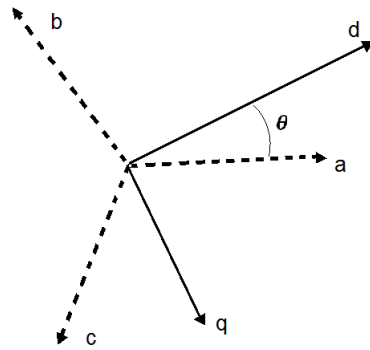


Figure 2.3: The rotor and stator reference frames

in many of the PMSM machines, the difference in the air gap flux is not high enough to be used for position estimation. Depending upon the saliency of the motor, the solution for control of PMSM will differ. Only a non-salient type will be considered in the thesis since the proposed solution aims at sensorless control of non-salient PMSM.

As shown in Fig. 2.3, the orientation of the 'd-q' axis depends on angle θ . This angle is used in the Park transform to obtain the 'd-q' frame voltages and currents[23]. The voltages(V_d, V_q), currents(I_d, I_q), resistance(R_d, R_q) and inductances(L_d, L_q) obtained by such transformation are represented in circuits shown in Fig. 2.4.

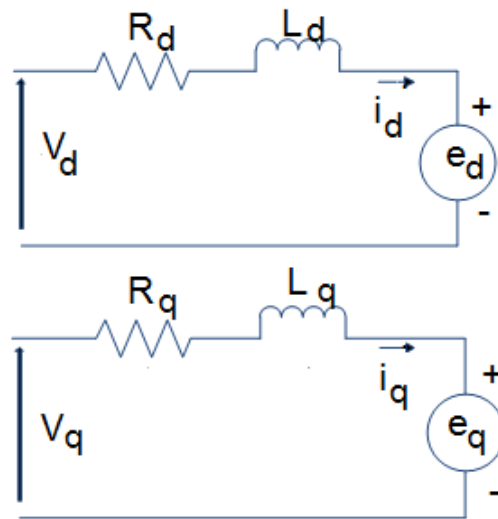


Figure 2.4: PMSM equivalent circuit in d-q axis

2.3.2 Motor model on the stator reference frame

The model based on the stator uses values which are directly measured from the motor's terminals. Each of the three stator windings can be modeled as shown in 2.5. Thus

there are three such circuit model for a motor, each representing a phase of motor. The time domain voltage equation of the each phase of the motor is obtained by applying Kirchoff's voltage law in the circuit shown in Fig. 2.5 (Eq.2.1)[30].

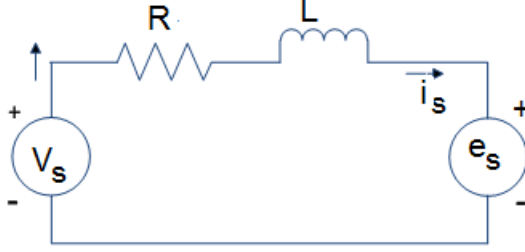


Figure 2.5: PMSM equivalent circuit of stator side

$$V_s = R \cdot i_s + L \cdot \frac{di_s}{dt} + e_s \quad (2.1)$$

V_s, i_s, R, L represents voltage, current, resistance and inductance respectively for each of the three phases of the stator windings. e_s is the back EMF voltage. Rearranging the terms in the equation 2.1, equation 2.2 is obtained.

$$\frac{di_s}{dt} = \left(-\frac{R}{L}\right)i_s + \frac{1}{L}(V_s - e_s) \quad (2.2)$$

The above equation in digital domain of a controller which samples the current and voltage values is given in equation 2.3 [31].

$$\frac{i_s(n+1) - i_s(n)}{T_s} = \left(-\frac{R}{L}\right)i_s + \frac{1}{L}(V_s(n) - e_s(n)) \quad (2.3)$$

Where T_s is PWM loop time.

$$i_s(n+1) = \left(1 - T_s \frac{R}{L}\right)i_s(n) + \frac{T_s}{L}V_s(n) - e_s(n) \quad (2.4)$$

$$= F \cdot i_s(n) + G \cdot (V_s(n) - e_s(n)) \quad (2.5)$$

$$\text{where } F = \left(1 - T_s \frac{R}{L}\right) \text{ and } G = \frac{T_s}{L} \quad (2.6)$$

The motor parameters F and G need to be calculated from the R and L values of the motor. The stator currents are converted from three stator components (I_a, I_b, I_c) to two rotating components (I_α, I_β) by Clark transform[23]. With the latest high speed digital signal controller the Clark transform can be implemented very efficiently.

2.4 Conclusions

From the modeling of the PMSM in both the stator and rotor reference frame it can be concluded that the stationary frame model require transformation of stationary value to

rotating frame. The process of transformation needs the angle or rotor position. The d-q reference frame can be obtained with the use of powerful digital signal controller that can do the transformation very fast. Since the transformation requires the angle value, accurate estimation of the angle is a requirement for control in rotating reference frame. In the case of sensorless control, the angle has to be estimated within a model of motor using the current inputs and then used in the transformation step.

Sensorless Algorithms for Motor Control

3

The chapter covers some of the algorithms proposed in the past for the motor control with sensorless schemes. In section 3.1 the surveyed solutions were classified into different categories based on various criterions. Section 3.2 describes the major algorithms for the sensorless control. A comparison between all the described schemes is then presented in section 3.3. Finally the conclusions from the survey are presented in section 3.4.

One of the earliest research papers on controlling synchronous motor without shaft sensors was published in 1979 by Allan B Plunkett and Fred G Turnbull working in the power electronic lab of General Electric [24]. It uses torque control based on the estimation of the phase angle between the voltage and current. The calculation was done with the circuit blocks available then. The calculation was divided into different blocks with the output of each circuit block as input to next stage. In 1985, a 4-bit single chip microcomputer was used for the sensorless speed control for controlling brushless motor[9]. The minimum speed achieved for that solution was 2000rpm. The unique feature of this solution was that the control was implemented in software and it was used to get the desired PWM frequency to achieve speed control. Following this solution many control strategies were proposed based on different features of motors. The minimum speed for control was brought down to some extent with improved back EMF estimation. The different schemes which were proposed by later research papers are discussed in the coming sections.

3.1 Classifications

The solutions that were proposed previously for sensorless control varied in its application, complexity and accuracy. They can be classified based on many criteria as given below.

Based on the type of motor used in controlling scheme there can be two classification.

- (i) Surface mounted permanent magnet motor (SMPM)[17]: In these type of control solution the motor used for control is of surface mounted type. The variation of inductance is less as the rotor position changes.
- (ii) Interior rotor permanent magnet (IPM)[17]: In these type of control solution the motor used for control is of interior mounted type (IPM). In case of the IPM the inductance of stator winding varies with rotor position creating imbalance in the phase impedances and variation in neutral voltages.

Based on the requirement of rotor position in motor control, the solutions can be classified into two [6][7].

- (i) Absolute rotor position estimation: In this type of motor control the exact position of the rotor is essential for the control scheme. The rotor positions is either directly measured or estimated using current inputs. e.g., saliency tracking.
- (ii) Relative rotor position estimation: In this type of solution the position is not needed for motor control, instead the torque on the motor is calculated and maintained to the achieve set speed.

Based on the dependency on the motor parameters there can be two classification [25][3].

- (i) Parameter dependent: In this type, the controlling schemes depend on the motor parameters such as stator resistance and stator inductance. Methods such as current observer, fish method, INFORM are parameter dependent. Similarly, methods based on stator flux and torque control loops depend on motor parameters. They are sensitive to stator resistance at low speeds.
- (ii) Parameter independent: In the second type of classification the controlling solution depends on the motor parameters. Methods such as Kalman filters and saliency tracking do not depend on motor parameters [33][3].

3.2 Main sensorless schemes

Some of the best existing solutions of sensorless Field Oriented Control (FOC) were studied in detail to get a better understanding of the challenges faced with the low speed control. It also provided the general approach to various kinds of motors and the useful features could be adopted for the sensorless scheme to be implemented. Some of the studied solutions are given bellow.

1. Extended Kalman filter [33].
2. Saliency tracing [3].
3. Fish method [29].
4. Current observer [31].
5. INFORM method [25].
6. Magnetic Anisotropy [22].
7. Current observer improved [28].

A brief review of the main solutions is presented in the next section.

3.2.1 Kalman filter solution

The solutions based on the Kalman filter are discussed in [33], [10] and [2]. The solution essentially involves Kalman filter applied to non linear system. The systems equations are solved for its unknown parameters by iterative operations on the system variables using matrices. The matrices need to be tuned based on the errors and noises in the measuring circuits.

One of the main advantages of Kalman filter is that it does not require the motor parameters or the initial position of the motor. However the tuning of matrix values to get a stable system was too challenging to be finished within the time frame. On a business perspective this technique did not give the optimum returns for the time and effort that needed to be put. Hence this method was not considered for the sensorless solution.

3.2.2 Saliency tracking method

Salient pole AC machine have difference in inductance along the d and q axis of motor. This is called the saliency of motor. The methods based on the saliency require superimposition of a high frequency signal over the fundamental stator current component. The high frequency signal cause high frequency current in the motor whose amplitude depends on the rotor position. The high frequency currents are filtered using a band pass filtered and position is estimated. However these methods sometimes require a very high PWM frequency for implementation [3][4][11]. They have the following advantages.

1. Estimation can be used for all ranges of speed. Control is possible for speeds ranging from zero to very high speeds.
2. No additional hardware is required for voltage injection (same inverter can be used) and signal demodulation.

However, they have the following disadvantages.

1. Rotor position is estimated from saliency, which is not present in all the motors.
2. In motors without saliency, additional steps need to be taken to create saliency feature. This involves changing the motor design slightly to induce saliency feature.

It was decided after the study that even though the accurate way for solving sensorless would have been saliency tracking its application will involve tampering with the motor design. Therefore a method based on saliency was not suitable for the required sensorless FOC solution.

3.2.3 Fish Method

In this method the current and stator flux are projected to the rotating frame [29]. The analysis of the two curves obtained in the rotating frame is then used for speed control. The shape of fish flux is determined by the overall effects of the higher harmonics combined. The ratio between the current and flux values gives the values of the inductance.

The distortion between the flux and current waveforms reveals the information about the motor parameters.

This method can be applied to non salient motors as well. It has full range of operation from zero speed onwards. Compared to Kalman filter the only disadvantage is the requirement of stator resistance for standstill operation. Being a patented solution this method was not chosen for further study and improvement.

3.2.4 Current observer

The current observer differs from the previous methods because of its method of estimating position and speed of rotor. The angle and speed is estimated by observing the stator current and using it in a motor model. The error in the model is corrected with the iteration process and the back EMF values are estimated from the model. The EMF values are further used for angle and speed estimation. However the solutions current observer method can only be used only for speeds above a minimum limit. Below that speed the back EMF estimated from the motor model is too small to be used for getting the position correctly [31][14]. Another disadvantage is that torque control at low speed was not possible because of estimation errors at low speed.

3.2.5 INFORM method

This is used on machines that show self or induced anisotropy [25][32]. This method relies on the measurement of variation of the rotor current which is based on its inductance value. This will give the online reactance and the position of the rotor. While the measurement is done the main excitation has to be stopped to since in inductor the current will continue to flow even when the excitation is zero. However this method is suitable only for zero and low speed. At high speed the some other techniques like current observer or Kalman filter is required.

3.2.6 Magnetic Anisotropy

The method of magnetic anisotropy is a lot similar with the saliency method described before. However the anisotropy phenomenon is the property of the magnets inside the motor [22]. They acquire this property during their manufacturing process. The dipole in the magnet will align in a particular axis called easy axis. The axis perpendicular to this is hard axis. This will affect the magnetic field in which the motor is rotating. The anisotropy will cause a small change in the flux according to the rotor orientation. Measuring this effect will give the position and speed estimation.

However just like the saliency tracking this technique also not feasible because of hardware modifications required. Also it cannot be used on all kind of PMSM motors. The rotor parameters need to be known before for estimation.

3.2.7 Current observer improved

The improved current observer has the benefits of current observer previously explained. Apart from that at low speed the current injection will give a much better control of

torque when the angle estimation is not very accurate [28]. The described solution is using a stator reference frame to estimate the position and speed. If this solution can be adapted to rotor reference frame and if speed control is achieved instead of torque control then improved current observer is very ideal for sensorless vector control.

3.3 Combination of Solutions

Apart from the 7 solutions mentioned above some possible combinations of methods were also analyzed. This was done to check if the combination of solutions yield any new advantage.

- Current observer with INFORM
- Current observer improved with sampling and averaging
- Extended Kalman filter with sampling and averaging.

Each of the combination above is found to be better than their individual solution. A comparative study of all the main solutions and combinations is done in next section. For methods such as fish method, magnetic anisotropy and saliency tracking, combinations were not possible because they were not compatible with other's methods.

3.4 Comparison of the different methods

To make a comparative study of all the control schemes 11 criteria were selected. Weights were assigned based on the positive impact of each of the criteria. These criteria are explained below.

1. No special requirement of motor: If the saliency feature of motor is required for the control scheme.
2. No hardware parameter required: Some of the algorithm such as Kalman require the information about noise levels in the sensing hardware to tune the parameter in the control algorithm .
3. Motor parameter required/used: If the parameters are required then the control scheme has to be calibrated every time it is used for different kind of motor.
4. Propagation delay influence on accuracy: The algorithms which required a superposition of signals on the fundamental excitation had the issue of propagation delay in their implantation.
5. Is there additional Voltage or current injection: The voltage or current injection were given the least weight because this only meant.

6. Efficiency: The power consumed for the control strategy is very high priority. The efficiency should not be affected by the control strategy.
7. 20kHz PWM sufficient: The frequency of the injected voltage or current puts constraint on the PWM requirement. Since the PWM is a test bench hardware constraint it was given average weight.
8. Full range of speed possible: This is the highest weight of all the criteria since the sensorless has to work for speeds ranging from zero to high speed theoretically.
9. CPU load: This criterion is to know the CPU load that each algorithm puts on the controller. Since the controller CPU power is very high this criteria got very less weight.
10. Load torque estimation: Even at the low speed control to have the torque control is an advantage for the control scheme. This is important when the load varies on the motor.
11. Position accuracy: This is a criterion when the position of the rotor is required to be very accurate. In the current application it is not given the high priority.

Points were given on a scale of 0 to 10 for each criteria. The average of points scored in all criteria is used to get the final score of each method. The results of the comparisons are shown in the figure 3.1.

3.5 Conclusions from the survey

From the comparative study one can conclude that Fish method, Kalman filter with sampling and averaging, current observer with sampling and averaging are three best methods. Among these, Fish Method is a patented method and could not be used for achieving sensorless solution. The next best method of approach was Kalman filter. The Kalman filter involved the tuning of current sensors and creation of tuning matrices. The chances of completing this solution within a year was very slim. Thus the current observer with sampling and averaging was chosen as the method that will be taken up for vector control. Methods such as those based on neural network were omitted from study because of their complexity and longer implementation time.

Methods such as DFC (Direct Flux Control) were removed from consideration because of the type of motor used. DFC required access to the neutral point of the motor windings[21]. In the case of test motor used for this thesis access to neutral point is not possible. Apart from DFC, the techniques which are based on the reluctance motors were not considered since the test motor is not reluctance motor. However, motor controls based on reluctance property are useful for future application. It is predicted that in future magnetic materials will become costlier[18].

The solution to be implemented for the sensorless control of PMSM in this thesis is based on the improved current observer. As shown in the Fig. 3.1 it has the following advantages.

Criteria	Weight										weighted average of all scores		
	10	6	4	2	1	8	4	10	3	8		4	60
1 Extended Kalman filtering	10	0	8	10	10	10	10	10	10	2	9	7	8.1
2 Saliency tracking	0	10	10	0	0	10	10	10	10	0	5	3	4.8
3 Fish method Patented	10	10	5	10	10	10	10	10	10	3	8	9	9.0
4 Current observer	10	10	0	10	10	10	10	10	10	10	2	5	6.3
5 INFORM	0	10	0	0	0	10	10	10	10	4	5	6	4.3
6 Magnetic anisotropy	0	10	0	0	0	0	0	0	0	0	5	3	3.1
7 Current observer improved	10	10	0	10	0	0	5	10	10	8	7	7	7.5
8 INFORM+current observer	0	10	0	5	0	10	10	10	10	3	9	7	6.7
9 Current observer improved +Sampling and averaging	10	10	0	10	0	7	10	10	9	7	8	9	8.1
10 Extended Kalman filter +Sampling and averaging	10	0	8	10	10	10	10	10	10	1	10	9	8.4

Figure 3.1: Comparison of various sensorless control strategies

- No special requirement of motor.
- No hardware parameters required.
- Propagation delay does not influence the accuracy.
- Efficiency is better than other methods.
- 20kHz PWM is sufficient.

Current Observer Sensorless Scheme

4

Current observer based Sensorless Scheme was chosen as the sensorless scheme for this thesis. This scheme uses field oriented control (FOC) for motor control [31]. This chapter describes the current observer based sensorless scheme for motor control in detail. The different blocks in current observer are described in the section 4.1. In Section 4.2 the observer block in the current observer scheme is explained. Section 4.3 gives the advantages of this FOC scheme. Finally the conclusions are given in Section 4.4.

4.1 Sensorless FOC with back EMF estimation (current observer)

The phase currents of a motor i_a , i_b and i_c along with the rotor position(θ) are the inputs for FOC [9]. After processing these inputs, the sensorless FOC generates the three phase reference voltages V_a , V_b and V_c . The reference voltages are then used to drive the motor.

Some of the earliest motor control were implemented with scalar motor control in which the generated sinusoidal wave's frequency and voltage are varied on each of the three phases [7]. The speed of the motor was measured and fed back into the control loop. The models used for such control had validity only in the steady state. This greatly affected the efficiency of the motor since this resulted in transient spikes. All the controls were working on sinusoidal variable. As the speed of motor is increased, the frequency of system increases. This required the tuning of controllers at high speeds to have stable outputs. In systems which worked in a wide frequency range it was not possible to have a stable controller throughout the speed range.

Additionally, when such control mechanisms were used, technology was not advanced enough to measure the instantaneous current in the armature windings. With the availability of faster and more precise ADCs in the digital signal controller, it was possible to measure the line voltages and current instantaneously. Thus the motor drives were not bulky as before and were faster and less power consuming [24].

4.1.1 Space vector for three phase circuit systems

The use of space vector in representing the current and the voltage in the synchronous motors considerably eases the handling of three phase systems [23]. The general form of space vector is given by the equation 4.1.

$$\vec{X} = K(P_R + P_S.\alpha + P_T.\alpha^2) \quad (4.1)$$

Where $\alpha = e^{j\frac{2\pi}{3}}$ and $\alpha^2 = e^{j\frac{4\pi}{3}}$. P_R , P_S and P_T represent the instantaneous variables on three different phases. The constant K is a scalar whose value determines the final

magnitude of the vector. These values are constant and real. The space vector \vec{X} has a real and imaginary part as shown in equation 4.2 and Fig. 4.1.

$$\vec{X} = X_\alpha + jX_\beta \quad (4.2)$$

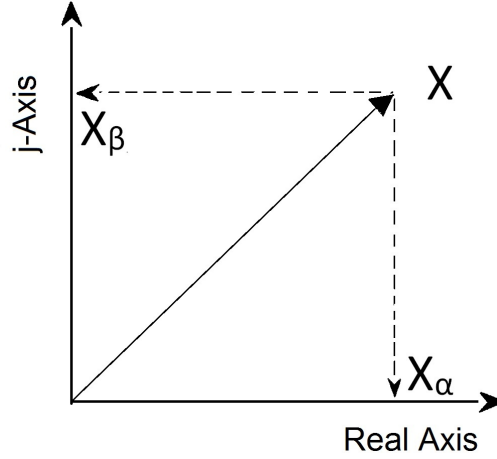


Figure 4.1: The space vector representation of two phases in complex plain (real and imaginary axis).

With the transfer of three phase values to two phase, the control is transferred to a two coordinate (d and q axis) time invariant system. Therefore it is always better to convert the star connected three phase circuit of motor to its space vector for better control mechanism. The circuit is modeled from the stator side using the space vectors. Fig. 4.2 shows the currents in the three phases of a stator. \vec{i}_s is the vector sum of the three phase currents. The three phases of the star connected synchronous motor can be described by the equations 4.3 to 4.5 [31]. The equations are obtained by applying Kirchoff's voltage law to the circuit in Fig. 2.4 [31].

$$V_{Sa} = i_{Sa}R + L \frac{di_{Sa}}{dt} \quad (4.3)$$

$$V_{Sb} = i_{Sb}R + L \frac{di_{Sb}}{dt} \quad (4.4)$$

$$V_{Sc} = i_{Sc}R + L \frac{di_{Sc}}{dt} \quad (4.5)$$

V_{Sa} , V_{Sb} and V_{Sc} are the phase voltages while i_{Sa} , i_{Sb} and i_{Sc} are the phase currents. R and L are the phase resistance and phase inductance respectively. The three equations can be rewritten in the vector form as equation 4.6.

$$\vec{V}_{Sabc} = \vec{i}_{Sabc}R + L \frac{d\vec{\psi}_{Sabc}}{dt} \quad (4.6)$$

Where $\vec{\psi}_{sabc} = L \vec{i}_{sabc}$

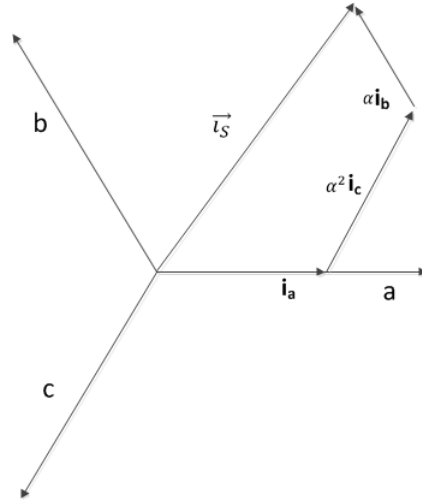


Figure 4.2: Space vector representation of current vectors in three phases.

This model can be used to generate the space vector of \vec{i}_{s123} . First the input vector \vec{V}_{abc} is resolved into its two components $V_{s\alpha}$ and $V_{s\beta}$. $V_{s\alpha}$ and $V_{s\beta}$ are the two phase representation of the stator voltages. These are then used to calculate the scalar variables $i_{s\alpha}$ and $i_{s\beta}$. Then using two to three phase conversion module the phase currents i_{sa} , i_{sb} and i_{sc} are obtained. Fig. 4.3 shows two phase representation of phase currents.

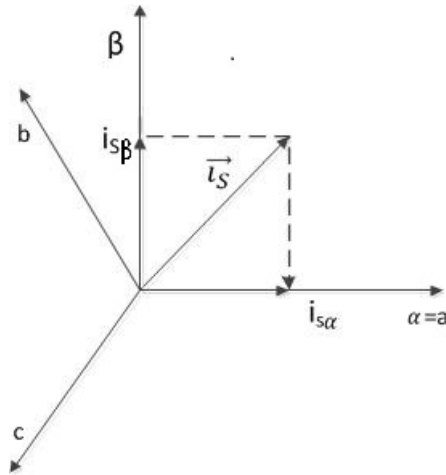


Figure 4.3: Three phase to two phase conversion of vectors

The Clark transform used to convert the three phase system into two phase system[1] is given below.

$$i_{s\alpha} = i_a \tag{4.7}$$

$$i_{s\beta} = \frac{1}{\sqrt{3}} \cdot i_b + \frac{2}{\sqrt{3}} \cdot i_c \tag{4.8}$$

The two phase system obtained by Clark transform is still a time and speed dependent system. This system is referenced on the stator frame. This system is transformed to the rotor reference frame by the projection shown in Fig. 4.4. In space vector control it is possible to model the three phase circuits in same way as single phase circuits. Thus it is used to model the three phase synchronous motors to simplify the process.

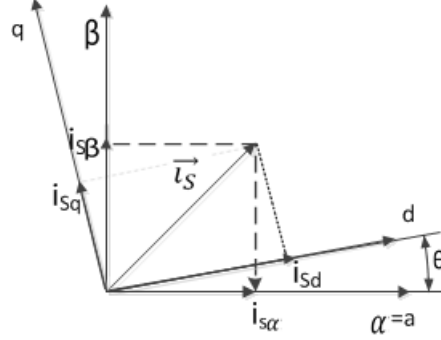


Figure 4.4: Projection of two phase stationary frame to rotating (d-q) frame.

The projection done in Fig. 4.4 is called Park transform[1][8]. Here θ represents the rotor position. The Park transform used to obtain i_{sd} and i_{sq} is described by the equations 4.9 and 4.10

$$i_{sd} = i_{s\alpha} \cos \theta + i_{s\beta} \sin \theta \quad (4.9)$$

$$i_{sq} = -i_{s\alpha} \sin \theta + i_{s\beta} \cos \theta \quad (4.10)$$

i_{sd} and i_{sq} are the two phase rotating components of the total current applied to the system. i_{sd} is used to control the flux in motor and i_{sq} is used to control the torque of the motor. The new two-co-ordinate system (d-q) is a time invariant system[5]. It is possible to directly control the torque by adjusting the flux and torque components.

The estimated and actual values of i_{sd} and i_{sq} are compared to calculate the reference voltages V_{sd} and V_{sq} to be applied in the d and q axis respectively. The two PID blocks shown in Fig. 4.5 are used for this purpose. The output voltages of these PID blocks are used to calculate the reference voltage V_α and V_β in the two phase system in the stator. The inverse Park transform used for this transformation is given in equation 4.11 and 4.12 [8].

$$V_{s\alpha} = V_{sd} \cos \theta - V_{sq} \sin \theta \quad (4.11)$$

$$V_{s\beta} = V_{s\alpha} \sin \theta + V_{sq} \cos \theta \quad (4.12)$$

Thus, two reference voltages are obtained to be applied on the motor. The steps taken to arrive at this reference voltages are summarized below.

- The phase currents I_a and I_b , (calculate I_c , $I_c = -(I_a + I_b)$) are obtained.

- Clark transform is used to obtain the two phase system.
- Park transform is used to get the rotating frame currents i_d and i_q . These are constants at steady state value.
- Once the I_{sd}, I_{sq} and the reference values of each is obtained then the error signals is generated.
- The error values are passed through PID (Proportioanl-Integral-Differentiator) controllers to get V_{sq} and V_{sd}
- V_{sq} and V_{sd} are transformed to the stationary frame using the inverse park transform.
- Subsequently inverse Clarks transform is used to get the three phase voltages V_a, V_b and V_c .

Fig 4.5 shows the various steps of the FOC scheme explained before. The Block SV-PWM generates the PWM signals for the voltages V_a, V_b and V_c .

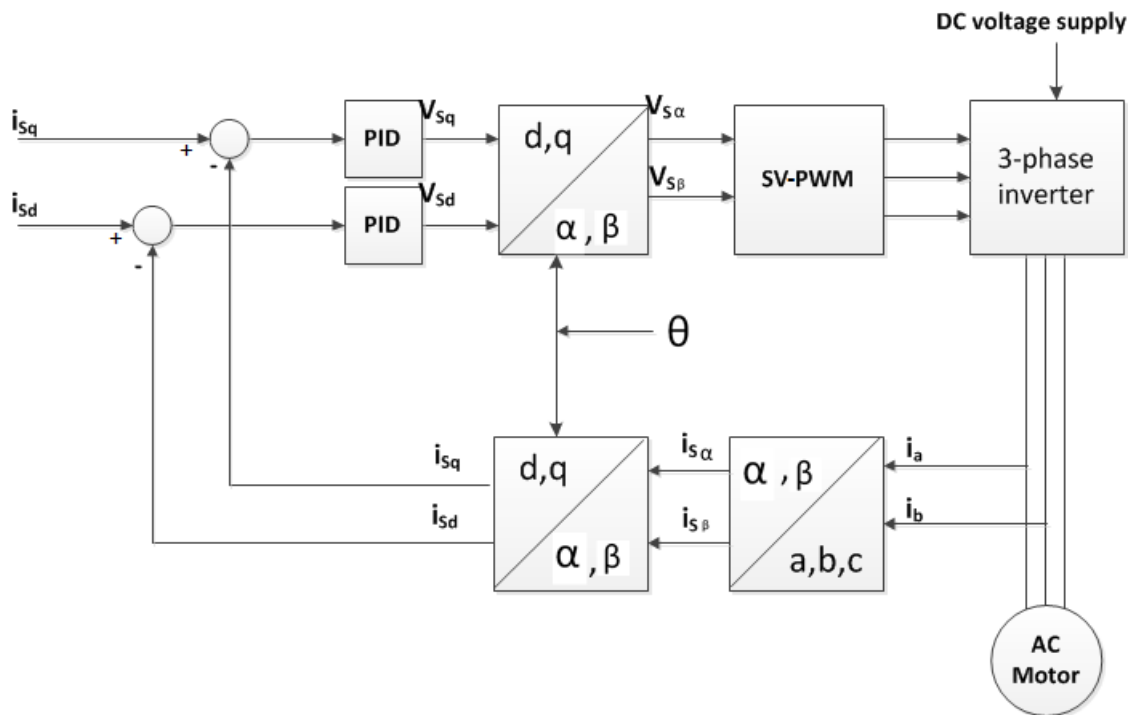


Figure 4.5: Basic FOC scheme. Angle theta is obtained from an observer block in a sensorless scheme[8].

From Fig. 4.5 it is clear that, apart from the two phase currents, the FOC scheme requires the rotor position or angle information. For a synchronous machine the rotor flux angle θ is same as the position of the rotor and it can be calculated by sensors which give the position of shaft. In sensorless scheme the angle θ has to be estimated by observer block given in Fig. 4.6.

4.2 Observer Block

The θ in Fig. 4.5 is calculated in the observer block of algorithm shown in Fig. 4.6. The observer block takes the two phase stator current ($I_{s\alpha}, I_{s\beta}$) and voltage ($V_{s\alpha}, V_{s\beta}$) as inputs. The outputs of the block are estimated shaft angle and rotor speed.

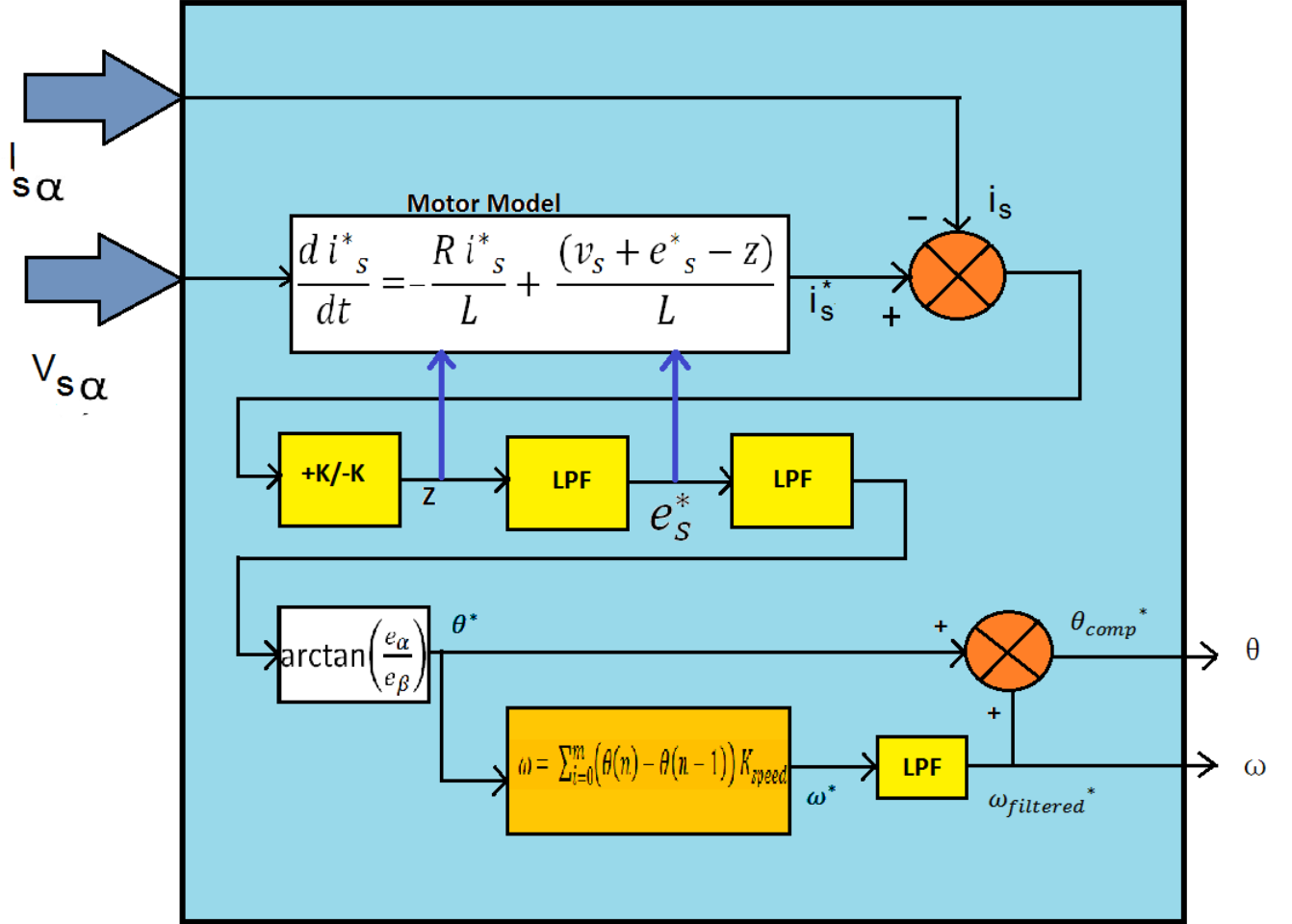


Figure 4.6: Observer block with motor model, slide mode controller, low pass filters(LPF), angle compensation.

The observer has a slide mode controller(+K/-K) that processes the error of estimated and measured currents. It has a motor model which is used to calculate the current. The estimated current i_s^* is then matched with the measured current i_s . When both the estimated and measured currents are the same then the EMF in the model is used for the actual EMF. This way the EMF is estimated. The time domain equations used in the model to represent the motor in 'two phase coordinate system' (α - β) are given below.

$$\frac{di_{s\alpha}}{dt} = -\frac{Ri_{s\alpha}}{L} + \frac{(V_{s\alpha} + e_{s\alpha} - z_\alpha)}{L} \quad (4.13)$$

$$\frac{di_{s\beta}}{dt} = -\frac{Ri_{s\beta}}{L} + \frac{(V_{s\beta} + e_{s\beta} - z_\beta)}{L} \quad (4.14)$$

z_α and z_β are the filtered error values where as $e_{s\alpha}$ and $e_{s\beta}$ are the actual back-EMF of the two phase systems. The functional blocks inside the observer are explained in the next section.

4.2.1 Slide Mode Controller (+K/-K)

The Slide Mode Controller (SMC) takes the input from the output of the comparison of the measured and estimated currents. +1 or -1 is generated first based on the comparison and it is multiplied with a factor k to get the output correction factor Z[31]. The gain is added to the voltage term of the digitized model and the process repeats until the measured and the estimates currents are the same. The correction factor that is obtained from the slide mode controller is then passed through the low pass filter (LPF) to get the EMF estimation. This is fed back to the model which gets updated every control cycle. The flow diagram of the observer is given in the appendix A.1.

Implementation of the low pass digital filter for the filtering the correction factor to get the Back-EMF is as follows[31]. If the input to the filter at sample number n is represented by x and the output by Y, then

$$Y(n) = Y(n-1) + k.x(n) - c.Y(n-1) \quad (4.15)$$

$$Y(n) = Y(n-1)(1-c) + k.x(n) \quad (4.16)$$

$$Y(n) - Y(n-1)(1-c) = k.x(n) \quad (4.17)$$

Applying z transform on equation 4.17 the following equation is obtained

$$Y(z) - Y(z)z^{-1}(1-c) = kX(z) \quad (4.18)$$

$$\frac{Y(z)}{X(z)} = \frac{k}{(1-z^{-1}(1-c))} \quad (4.19)$$

First order digital filter can be represented in the form of equation 4.20 [31].

$$Y(n) = Y(n-1) + 2\pi.F_c.T.(X(n) - Y(n)) \quad (4.20)$$

Correction factor z is the input X here and the filtered output e^* is obtained at Y(n). Therefore, substituting the input and output in equation 4.20 the following equation is obtained.

$$e^*(n) = e^*(n-1) + \frac{1}{F_{pwm}} 2\pi.F_c.T.(z(n) - e^*(n)) \quad (4.21)$$

where e = estimated EMF, F_{pwm} is PWM frequency at which the digital filter is being calculated. F_c = cutoff frequency of the filter, $Z(n)$ is unfiltered EMF from the output of the slide mode controller or correction factor.

The estimated EMF is used at two places.

1. In the model to calculate the current and match with the measured current.
2. In the calculation of the angle of rotation.

The angle is calculated by the following equation [17].

$$\theta = \arctan \frac{e_\alpha}{e_\beta} \quad (4.22)$$

Arc tan is calculated using CORDIC algorithm which is less expensive on the computation time. Once the angle is calculated, $\text{speed}(\omega)$ is derived from angle. Speed is calculated by adding the θ over m samples and then multiplying by a constant K_{speed} [23].

$$\text{Speed}(\omega) = \sum_{n=1}^m (\theta(n) - \theta(n-1)) \cdot K_{speed}$$

Where $\text{Speed}(\omega)$ = angular velocity, $\theta(n)$ = current theta value, $\theta(n-1)$ = previous theta value, K_{speed} = amplification factor, m = number of theta values added.

However, the angle calculated needs to be phase compensated because the filtering functions (LPFs) applied before its calculation create a phase lag. This compensation varies with the speed. Thus, angle compensation is a function of speed. New theta is calculated as

$$\theta_{compensated} = \theta + \theta_{offset}$$

where θ_{offset} is determined by the motor speed.

The space vector PWM block with inverters to supply the voltage to the three phases is implemented as shown in Figure 4.7. The ON-time of switches 1,2 and 3 in the figure are calculated based on the PWM signals from the controller. These switches are used to provide the calculated current from the power source V_{DC} .

4.3 Advantages of FOC

Vector control or FOC control gives a much improved performance compared to other controls. This control is characterized by smooth control over wide speed range, fast acceleration and zero speed torque control. The stator current is converted to two components magnetic field generating and torque generating. There will be two controlling loops for each of the components. The signals from the voltage and current sensors are used for the feedback into the loop. It requires the rotor position information which is

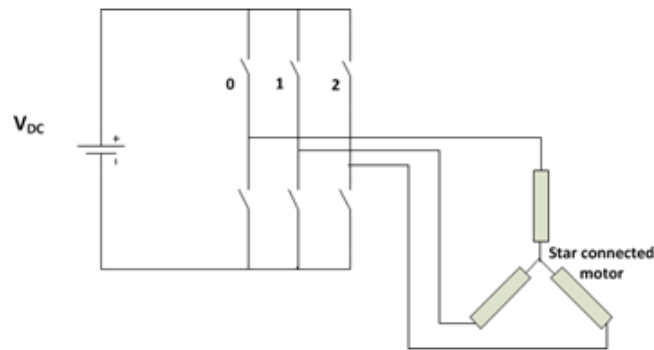


Figure 4.7: Space Vector PWM block

estimated. The rotor speed is calculated based on the rotor position captured at different time.

The three phase signals are converted to 2 phase by Clark transform to get rotating reference frame. The new calculated voltages are converted to stationary reference again by inverse park transform. After this it is converted to 3 phase components to be applied on the motor. Two separate PID (Proportional-Integral-Differential) feedback loops control the two components of the current I_{sq} and I_{sd} .

Limitation of FOC scheme is as follows

- It is cannot be used for zero and low speed estimation,
- Back EMF is very small at low speed and therefore the model is not accurate at low speed.
- Motor parameter variation affects the model accuracy.

Observer stability can be analyzed using rigorous control theory (Lyapunov stability) [6]. The observer can have different options while making the choice of model. The first choice is to make the estimations in stator or rotor frames. Both have its advantages and disadvantages. If the stationary frame is used then there will be little effect due to error of transformation angle on the speed estimation. At the same time this method of stationary frame reference has its own difficulties. In stationary reference frame the AC (Alternating current) signals need to be regulated by the controller. Most of the speed control solutions implement the use of slide mode controller. It has the advantage of effective regulation of AC and good robustness. However it also introduced ripples in the estimated speed.

If the observer is based on the rotor then it can be used for both salient and non salient motor since the inductance of stator is not varying when compared to the rotor inductance. So it is better to have the equation in rotor side while making the model. Also with rotor side, the d-q components can be separately controlled using PID control loops.

4.4 Conclusions

This chapter explored the working of a FOC based current observer scheme used for the sensorless speed control. The current observer based controlling scheme available in market do not work for low speed. At low speed, the back EMF is not significant enough and the observer cannot get the accurate estimation of the current. This leads to unstable and often wrong speed being estimated. If the shortcomings of the current observer can be overcome then this scheme with FOC can be used for low speed control.

Improvement in the sensorless scheme

5

In this chapter the current observer is analyzed further to look for the possibility of improvements at low speed. Sections 5.2 to 5.4 explain the different improvements suggested for current observer scheme. The conclusions from the chapter are presented in section 5.6.

5.1 Methods to improve current observer

It is found that the sensorless scheme in its current form was not efficient for the motor control at low speed. The lowest speed that the sensorless control was able to achieve was 450rpm. The ways to improve the sensorless at low speed were further explored. The main restriction with the current observer in its present form is lack of sufficient Back-EMF at low speed for the current observer to estimate the speed correctly. Therefore, improvements such as current injection, current averaging and voltage compensation were formulated to improve the low speed motor control. These improvements will be explained in the following sections.

5.2 Current injection

A method with the current injection for an observer based solution on a stator reference frame model was earlier attempted in a research [28]. However, in that research the motive was to compensate for the torque error by adding more current to field. In this thesis the speed control is achieved from the rotor reference frame. Therefore, a different scheme is necessary. The current injection applied for low speed is inspired from the field weakening method. Field weakening is one of the ways to make the sensorless control work for higher rated speed [13]. Using field weakening method, the motor could be rotated at speed larger than the rated speed with the same field excitation. In the field weakening method a negative current is injected into the d- axis to reduce the flux along the d-axis. This made sure that for the same speed the field excitation required would be less. The same concept can be used for achieving low speed control. However, the current injection will be done for the purpose of getting a measurable back-EMF signal at low speed. Thus, instead of injecting negative current, as in the case of field weakening, a positive current can be injected to d-axis. Table 5.1 gives the basic difference between field weakening and current injection.

- Flux along the d-axis is increased.
- The back-EMF for the same speed is now increased.

Applying Kirchhoffs voltage law on the stator side [17]

Table 5.1: Comparison between the field weakening and current injection

Field Weakening	Current injection
The negative I_d is injected	Injecting positive I_d current
Flus along the d-axis is reduced	Flux along the d-axis is increased
Used for high speed operations	Used for low speed operations

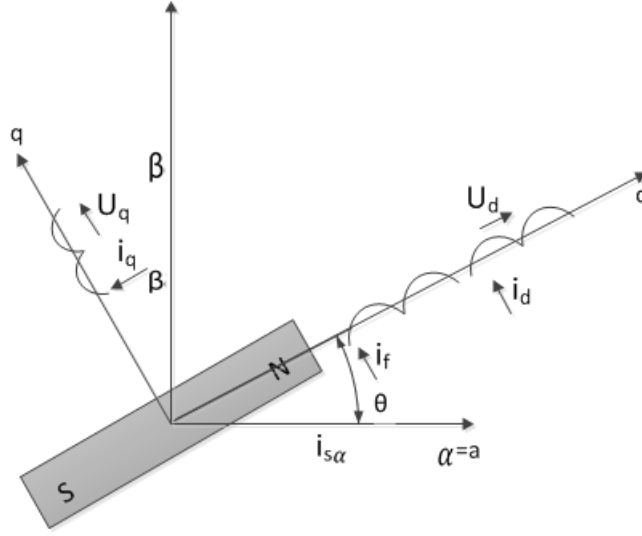


Figure 5.1: Synchronous frame of PMSM showing the currents causing the flux in the two axes.

$$V_s = I_s R_s + \frac{d\psi_s}{dt} \quad (5.1)$$

Where

$$\psi_s = I_s L_s + \psi_m \quad (5.2)$$

Similarly for the Rotor side

$$\psi_d = L_s I_d + \psi_m, \psi_q = L_s I_q \quad (5.3)$$

For simplification assume steady state, $L_s = 0$

$$\psi_s = \psi_m, \psi_d = \psi_m \quad (5.4)$$

The back EMF $\frac{d\psi_s}{dt}$ is then $\frac{d\psi_d}{dt}$

Therefore increasing flux along d-axis will increase the back-EMF. A higher and measurable back-EMF is necessary for the correct estimation of the angle and speed. Figure 5.1 shows the d-q axis with the magnet aligned along the d axis. The flux along

the two axes are caused by the currents shown. The currents which affect the flux ψ_d are i_f and i_d . I_f in the present solution cannot be changed because permanent magnet is used for field excitation. Therefore changing i_d remains the only way to increase the back-EMF. This is done in software by setting the i_d to the necessary value. The total current drawn by motor is given by equation 5.5.

$$I_m = \sqrt{I_q^2 + I_d^2} \quad (5.5)$$

Because the estimated speed will give a larger speed than actual speed by a factor proportional to the injected I_d , this new speed and angle has to be scaled down by a factor before using in feedback loop.

Thus current injection was one of the proposed ways to improve the sensorless scheme at low speed. The expression for the electromagnetic torque is given by the equation 5.6[30][8].

$$Te = \frac{3}{2}P(\psi_d I_q - \psi_q I_d) = \frac{3}{2}P(\psi_f I_q + (L_d - L_q)I_q I_d) \quad (5.6)$$

Beside the problem of very less or no back-EMF at low speed, the phase currents are sampled at a constant rate throughout the speed range of motor. This means that at low speed the controller is not optimally used. The controller can get a more accurate and noise free value if it processes the sampled value. This processing will not affect the speed control since the update rate will be less at low speed.

5.3 Current Averaging

For the speed estimation, the Back EMF at low speed is not accurate in current observer. The sampled current values are too small or inaccurate to estimate any derived values. To overcome this, the sampled values are added many times and averaged. Assuming the average noises cancel each other, the result will be a value that can be used in the back EMF estimation.

The sampling rate can be adjusted with the speed of the motor as shown in the equation below.

$$S_r = S_m - \frac{S_m - 1}{800}\omega \quad (5.7)$$

where S_m is the maximum sampling at the lowest speed. ω is the speed below which averaging the active. This scheme is expected to reduce the lower limit of the speed range. The limit up to which the sampling rate can be raised without affecting the speed estimation stability needs to be identified.

5.4 Voltage Drop Compensation

For the back EMF estimation the actual voltage across the stator is not used instead the calculated V_s in the previous step is used for the EMF estimation. The assumption here is that the voltage estimated V_s and the actual voltage applied on the motor is the same. Using the previous calculated V_s is favorable to eliminate the errors due to offsets

caused by the sensing hardware. However, the actual voltage and calculated V_s is not the same because of the inverter. Due to the drop across the inverter, the actual voltage on the stator is not the same as the calculated V_s which is the output of controller. The difference in this voltage will cause error in the speed control. To compensate this error, the output of the controller and the actual voltage on the stator is compared and an offset is added to the generated reference voltage.

The voltage drop across the inverters will reduce the actual voltage seen by the motor. At speeds closer to zero this voltage drop will be comparable to the voltage reference generated by the PWM signals. The MOSFETs used in the motor control (PSMN2R6-40YS) have a forward resistance of 3m which will cause the actual voltage across the motor to be slightly less. Schotky diode (PRL5819) used in the inverter stage has a forward voltage 340mV at .1A current rating. For 3A the drop across the diode is 900mV. These voltage drops need to be accounted for while generating PWM signals for the inverter stage. The compensation can be implemented in software with no additional hardware requirements.

This compensation scheme is not specific to low speed control. It could be used in general to improve the control scheme since the drop across the inverter is not restricted at low speed alone. The scheme is expected to remove the error from the estimation due to the inverter hardware and get more accurate speed estimation.

5.5 Integration of improvements into current observer

Based on the analysis given in the previous section the following three improvements were proposed.

- Injecting the voltage at low speed to improve the torque control at low speed.
- Having a variable sampling rate for the EMF estimation which will improve the accuracy at low speed.
- Having a voltage compensation to make sure the error in voltage at the stator does not affect the motor control at low speed.

The proposed improvements will be implemented in the existing current observer scheme. Topology of the new solution is given in the Fig. 5.2. In Fig. 5.2 the current injection scheme is implemented at 1. The block for current injection takes set speed as input and injects current into the d-axis. The averaging scheme is implemented at 2. The current averaging block changes the sampling size used for sensing the phase currents. The sampling size is determined by the speed input. The voltage compensation implemented at 3 will compensate the voltages based on the feedback of actual voltages.

5.6 Conclusion

Based on the study of the sensorless scheme three improvements were proposed. The current injection scheme which was inspired from the field weakening method used was

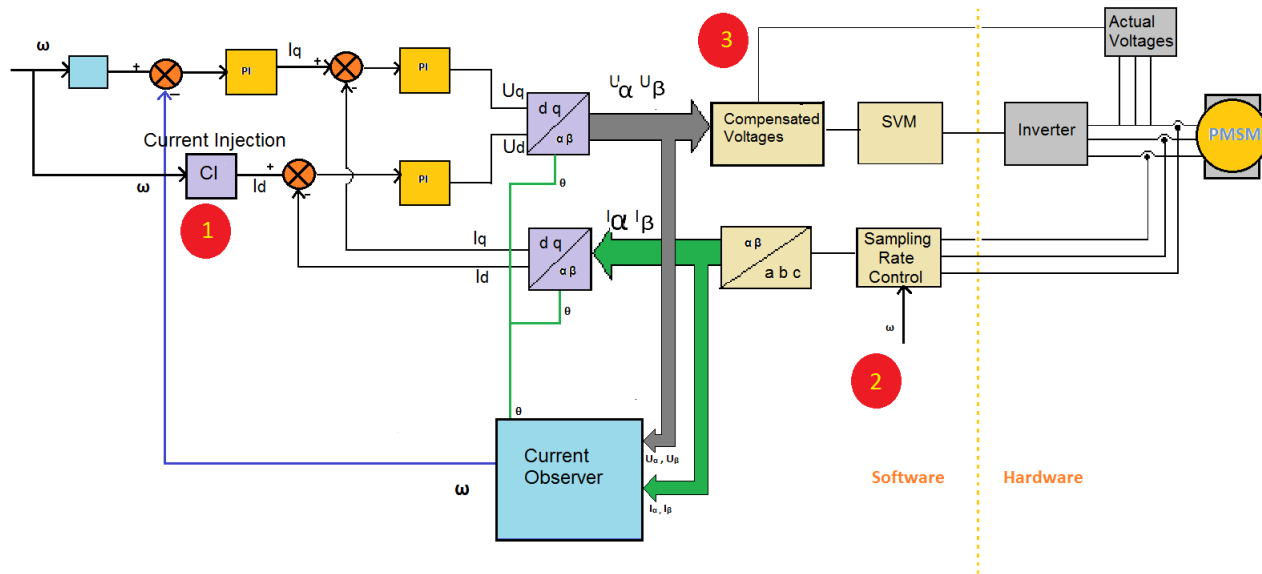


Figure 5.2: Improved Sensorless control block diagram

expected to achieve the maximum effect to achieve low speed control. The current averaging scheme is expected to filter the noise at low speed. The third proposed scheme of voltage compensation was found to be the least effective in achieving low speed control. Thus, the two schemes to be implemented on the sensorless scheme are current injection and current averaging.

Experimental setup and the implementation of proposed schemes

6

This chapter describes the experimental setup used for the design, testing and implementation of improvements in current observer. NXP's LPC 4350 microcontroller was used for the implementing the control algorithm. In section 6.1, the details of the LPC motor control board, tools used for the experiments, the motor used as well as the software tools is explained. Section 6.2 of this chapter describes the implementation of the current injection on the sensorless scheme at low speed. In this section the type of current injection and method to the arrive at injected current value is given. Section 6.3 of the chapter explains the implementation of current averaging scheme. In section 6.4 the conclusions of the chapter are given.

6.1 Experimental Setup

The experimental setup for the thesis includes the motor control board, power supply unit, programming tools, motor and the software for running and testing the algorithm. The experimental setup is shown in appendix A.2.

6.1.1 LPCXpresso motor control board

The LPCXpresso motor control kit is a platform for low voltage motor control based on NXP's controllers. It is possible to test different versions of the code and evaluate its performance. The board has following functionalities which makes the testing process easier.

- Phase voltage measurement: The terminal voltages of the motor (V_a , V_b and V_c) can be measured by the board.
- Phase current measurement: The phase currents (I_a , I_b and I_c) can be measured by the board.
- Over-current trip and break functionality: In the case of any over current the interrupt mechanism will send a break command to the motor. This will protect the board from over-current damage.
- Hall sensor and QEI (Quadrature Encoder Interface) sensor inputs: The correctness of the tested algorithm is verified by the QEI sensors.

The LPCXpresso controller board consists of the following functional blocks.

- **Power supply:** The board is supplied with a 24V, 2A power supply. There is 15W power supply on the board (+11V, +5V, +3.3V).

- **Controller:** The current is conditioned in the motor control board before being sampled by the ADC of microcontroller. The algorithm of sensorless control is executed in this controller. NXP's LPC1800 microcontroller is used for implementing the sensorless algorithm. The LPC1800 is a ARM Cortex-M3 based microcontroller. The ARM Cortex-M3 core offers many advantages such as low power consumption, enhanced debugging features. This series of microcontrollers operate at CPU frequencies of up to 150 MHz. The LPC18xx series includes up to 200kB of on-chip SRAM data memory multiple digital and analog peripherals. Two 10-bit ADCs with DMA support and a data conversion rate of 400 k Samples/s. Besides that it has UART ports which can be used for the debugging of the control algorithm and for testing.
- **ADC:** For the purpose of motor control the 10bit ADC of the LPC4350 is used for measuring the phase currents and Voltages. The ADC has a band width of 420 kHz. This means that it can be used to sample signals whose frequency are less than 210kHz. However if the ADC is oversampled then this frequency range can be further increased with some loss of precision. The accuracy of the sensorless speed is limited by the inputs precision. Thus it is essential to have an accurate phase current before processing it in software. The NXP's microcontroller used for the thesis has 10 bit ADC.
- **Memory:** The motor control board has an external flash which could be used for the program as well as internal RAM for debugging. For most part of the thesis the internal RAM itself was used for the testing.
- **PWM frequency:** The PWM is run at 20kHz frequency to generate the pulse which generated the sinusoidal voltage in the three phases.
- **Debug facility:** For the debugging of program a JLINK debugger tool is used. This was connected via JTAG to the motor control board.
- **Communication ports:** UART1, UART2 and serial ports are used for communication between the microcontroller on the board and computer.
- **Sensors:** The board can be configured for sensor inputs of Hall sensor or/and quadrature sensors. In the current project the quadrature encoder is utilized for running the motor during the development and testing stages of the thesis.
- **Data type and range:** The Data format of variable in the software is assigned according to their range of use and the accuracy required. The fixed point tool present in the motor control GUI is used for assigning the correct data type based on the range and precision of the variables.

6.1.2 Motor used for testing

For the purpose of testing the algorithm, a brushless DC motor which has sinusoidal back EMF is used. Table 6.1 gives the specification of the tested motor. It is a single pole pair motor which behaves just like a PMSM motor. Thus, it can be used for testing

Table 6.1: Specification of the motor.[20]

Power	80W
Nominal voltage	36V
Nominal Speed	132000RPM
Nominal current	2.06A
Starting current	19.7A
Terminal inductance	285.0uH
Terminal resistance	1.83ohm

the PMSM control algorithm. The motor has a quadrature sensor attached to it which can be interfaced to the controller for testing the algorithm's correctness.



Figure 6.1: A brushless DC motor

For a star connected load, the phase resistance and inductance is half of its terminal value. The phase inductances and resistances are calculated as $142\mu\text{H}$ and $.91\Omega$ respectively. These values are the motor parameter of the software in the controllers.

The power supply used for testing is a 24V supply. The rated nominal voltage of motor is 36V. Therefore, with the experimental setup the motor cannot be run at speeds greater than 80,000rpm. Since the motor is being tested for low speed this problem can be overlooked.

6.1.3 Software tools

Keil software was used for the writing the program and along with JLink was used for debug purpose. The UART connector was used to relay information back to the computer for viewing the program variable in motor control GUI(graphical User Interface) tool.

The motor control tool which was available in the NXP repositories was changed for the purpose of adding a new option of sensorless control. With the new option of sensorless control it was possible to test the algorithm from Motor control GUI. Besides that, additional variables in the algorithm were added to GUI for observation.

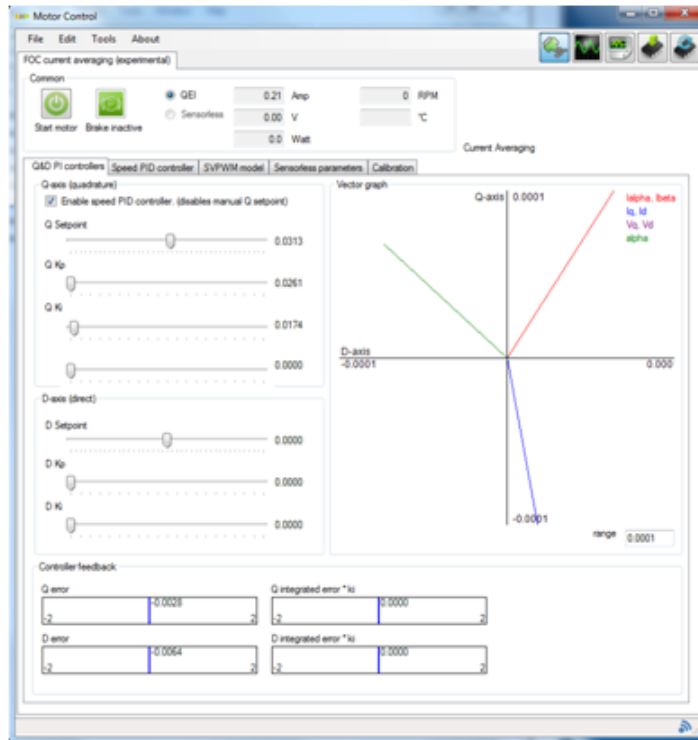


Figure 6.2: Motor control software tool.

The repositories in the NXP had the sensorless observer implemented for a different motor on a LPC2900 microcontroller. The sensorless code was first calibrated and rewritten for the motor under test. Then the improvements in the algorithm were implemented in the LPC1800/4500 microcontroller.

The quadrature sensors in the motor are used for getting the sensed speed value, which is compared with the test algorithm's speed estimation. The current observer was previously present in the software solution in the NXP repositories. However, the speed which was estimated by the current observer was not matching with the actual speed of the motor given by the quadrature sensors. Therefore the sensorless code required changes before it was used for testing. Once it was ready for testing, the proposed improvements in the scheme were added on it.

Figure 6.3 shows the software control flow. The inputs to the software such as D-axis reference current, Speed reference are set by user before the algorithm starts. Inputs such as phase currents and quadrature sensors are sampled during run time of algorithm. The software function has a main routine which contains a FOC loop that is executed when ADC is triggered. The current observer function is called in the FOC loop. The observer calculates θ and ω . These two outputs are further used to control I_d and I_q current variables. The output from the FOC loop is the three phase voltages V_a , V_b and V_c . The timing diagram for the execution of the algorithm is shown in Fig. 6.4. The

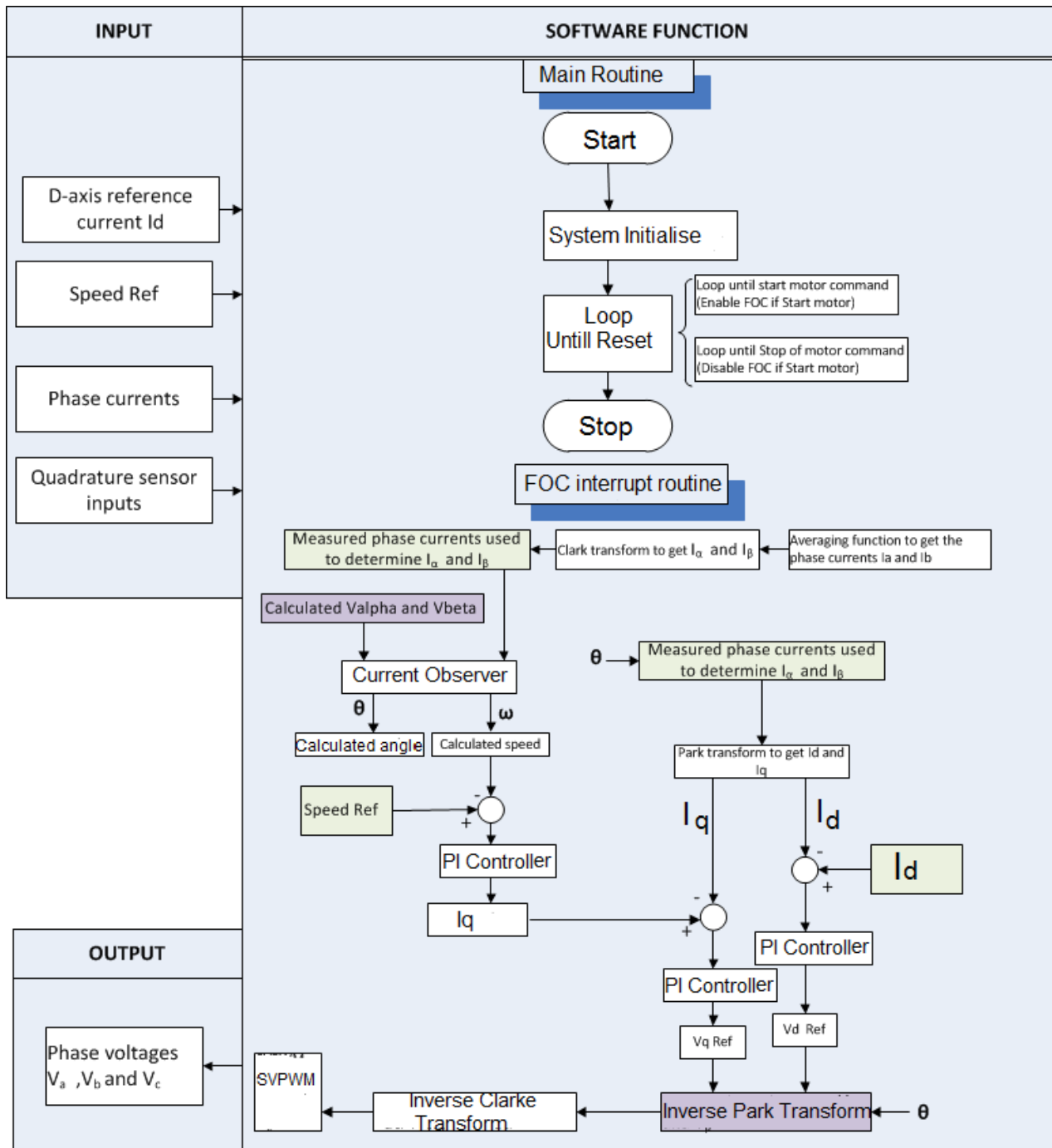


Figure 6.3: Software control diagram with input, functions and outputs shown.

ADC is triggered once in every PWM cycle. The time period for control loop is $50\mu s$. The algorithm should execute once and produce the outputs within this period.

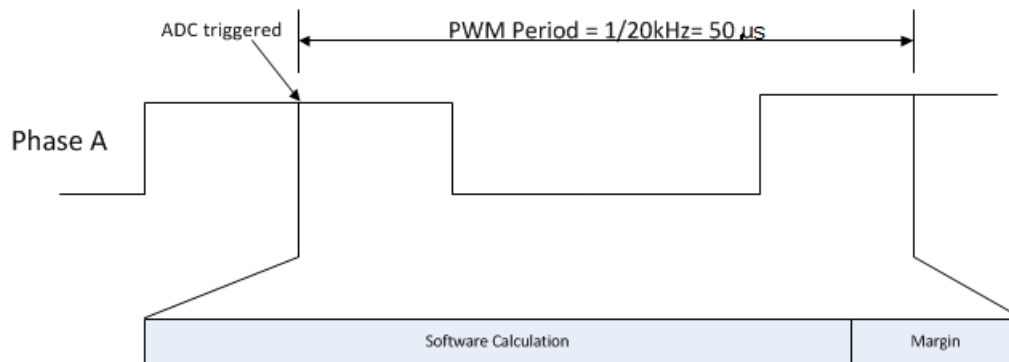


Figure 6.4: Timing diagram.

6.2 Current injection

The current injection scheme is expected to achieve the low speed control in the sensorless algorithm. The scheme has to be implemented on top of the sensorless solution. This integration requires testing and calibration which will be discussed in this section.

6.2.1 Steps for the implementation

The proposed current injection is to be implemented in the d-axis of the rotating frame. The value of current to be injected and the mode of injection need to be determined by experimentation as shown in Fig. 6.5. The procedure for arriving at the optimum value of the current injection as shown in Fig. 6.5 is described by the steps given below.

1. First, the effect of current injection on the back-EMF is quantified. This was done by injecting current into the d-axis by setting the PI controller of I_{sd} to a non-zero value in the software and measuring the voltage.
2. Compare the back-EMF (alpha and beta components) values with and without the injection. Find the function f_1 relating the current injected and the back-EMF change.
3. While calculating the estimated theta, offset compensation is added to get the correct value.
4. The d-axis current is injected when the motor speed is at low levels. The current is injected when the speed is less than w_0 (set during testing). Use EMF compensation while injecting current at various speeds. Find the function for which the injected current gives the control at various speeds. Plot the function $F = I(w)$ to be used for injecting current at different speeds.
5. Now create a new function for the change in back-EMF during current injection. Substitute this function in the compensation block in the flow chart (Fig. 6.5). Use the compensation whenever the current is injected ($w < w_0$). After testing adjust the injection of current at various speeds.

6. Test the current injection along with back-EMF compensation.

The above procedure was carried out for the current injection and it was found that the back-EMF compensation scheme was a constant. There was no error in the back-EMF estimation caused by the current injection. The back-EMF compensation block was therefore not necessary. Hence, the procedure was done for a fixed current injection and was applied only for speed control below 800rpm.

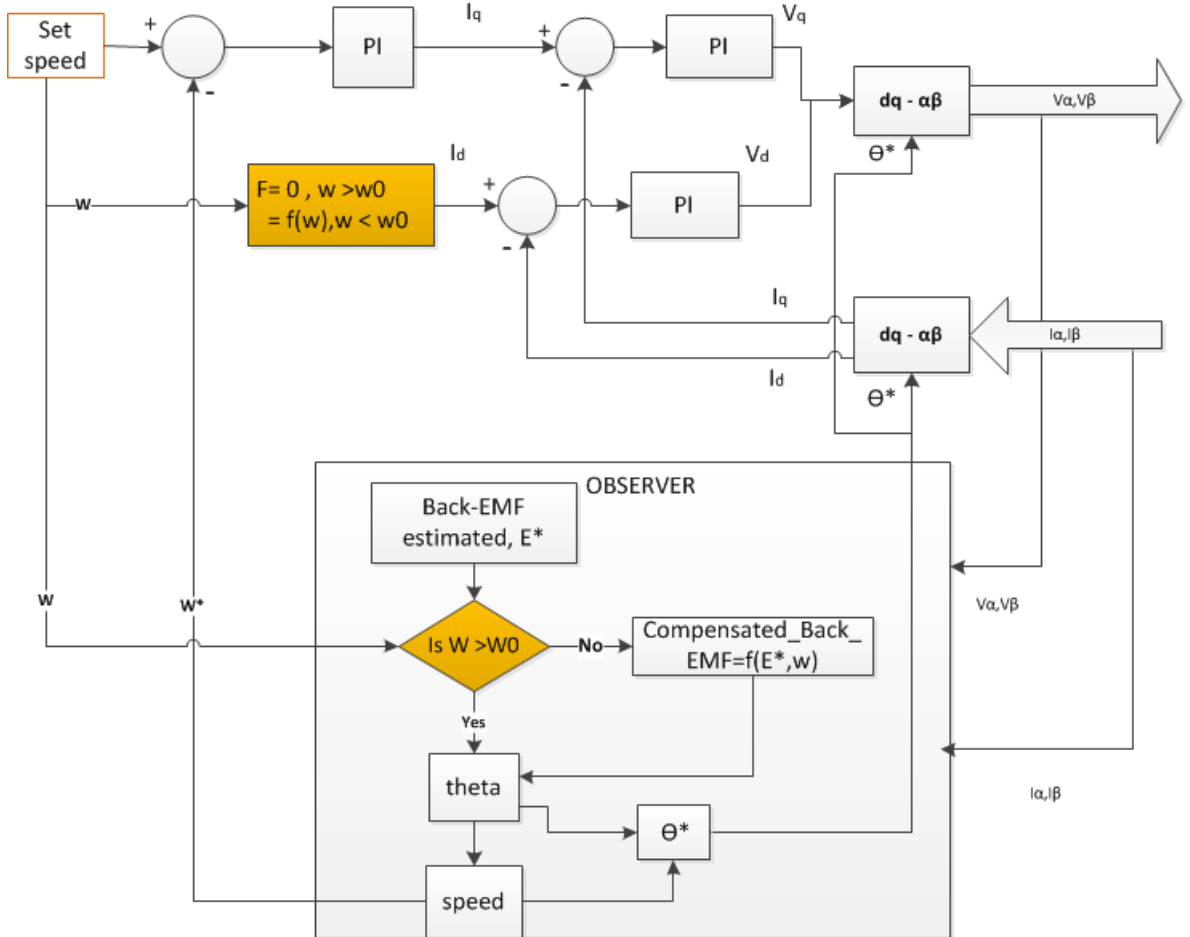


Figure 6.5: Testing scheme of Current injection.

6.2.2 Variation of current injection

The current injection should be done after knowing its relation function with the speed and the angle error. Once the error is identified and quantified in the algorithm the parameters of the current injection can be set either statically (before the start of motor) or dynamically (during run time). The standstill conditions need to be tested and incorporated to the algorithm to enable a startup routine. The startup routine should be having the ability to cover wide range of speed. The current injection method should

be stopped gradually as the speed increases and need to be completely stopped at the point where the back EMF estimation is sufficiently accurate for smooth operation of the motor. The equation of the injected current can be of two different type. In first type, the current injection will be varied as a function of speed as given in equation. In the second type, the function injects a constant current for speeds less than w_0 (w_0 is determined during testing stage) . The current injection of varying magnitude will have the following form.

$$f(n) = \begin{cases} i_0 - \frac{i_0}{w_0}|w| & \text{if } |w| < w_0 \\ 0 & \text{if } |w| > w_0 \end{cases}$$

It was found that the variation of current in the injection scheme was leading to more instability in the speed control. Thus, the use of fixed current injection was preferred for the scheme. Eventually, a constant i_0 is injected for speeds less than w_0 (800rpm) and no current injected for speeds above w_0 . After testing the current injection for various fixed values, the software variable of the scheme which injected the current was set to .00115. When the current variable was set to 0.00115 the speed response showed improvements at low speed. The PID values for the speed control was adjusted using ad-hoc method to minimize the speed error.

6.3 Current Averaging Scheme

This scheme is expected to improve the performance of the current injection at low speed because of the filtering feature of the averaging scheme.

6.3.1 The averaging scheme in signal processing

Averaging works like a low pass filter that removes the noises in the signal as shown in Fig. 6.6. The method of averaging can be used in combination with oversampling to have a higher resolution ADC. However, the ADC in the experimental setup is not oversampled in the time domain.

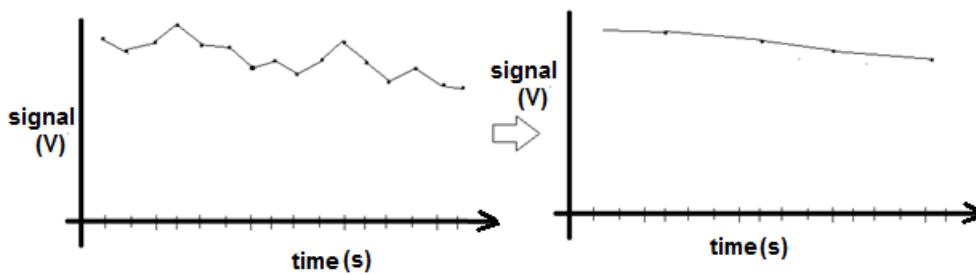


Figure 6.6: Averaging as a low pass filter. The output signal is smooth compared to input.

Here the purpose of the averaging method is to add small signals such as back-EMF to obtain a large signal. The large signal is noise free compared to the original signal. In

other words, the signal strength relative to the noise will be higher after averaging. The advantage of this will be noticed in the estimation scheme were the signal strength at low rpm is very small relative to the noise. This low signal strength can lead to an error in the angle and speed estimation. So improving the signal strength is very essential for the low speed sensorless motor control. The assumption here is that the noise signal is random and has a mean value of zero.

If the actual signal strength is denoted by S , the noise in the signal is represented by the standard deviation σ then after averaging n samples the new signal to noise ratio will be given by the equation 6.1 [26].

$$\text{Signal strength} = \sqrt{n} \frac{S}{\sigma} \quad (6.1)$$

As the number of samples(n) averaged increases, the signal strength also increases. An example of the averaging signals in the presence of noise is shown in Fig. 6.7.

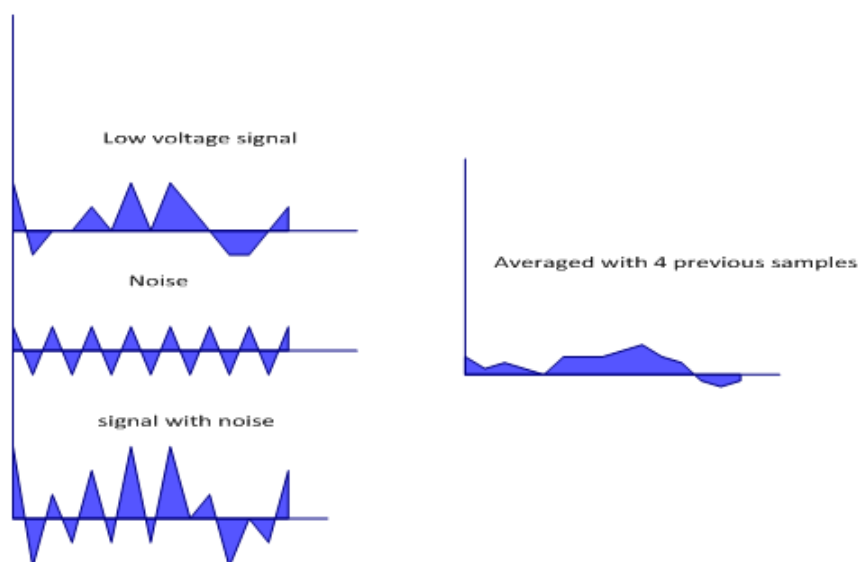


Figure 6.7: Low voltage signal with white noise averaged with 4 samples ($n=4$)

After the summation the sum is scaled to make sure that the unwanted bits are removed to get the correct result.

6.3.2 Implementation and results

The averaging was done as a function of speed. The averaging size n was chosen to be a power of 2. This was done so to make the division less time consuming for the controller. The division involved in averaging could be achieved by shifting bits by one position to the right. The size of averaging for various speed range was then found by experimentation. With the sampling size high at low speed it was expected to improve the estimation precision. The results of testing the averaging size is tabulated in Table 6.2.

Table 6.2: Speed range and averaging size used

Speed Range	Averaging size
0-200	64
200-250	32
250-325	16
325-400	8
400-450	4
450-475	2
above 475	1

6.4 Conclusions

The software control flow diagram for implementing the improvements was derived. A single value current injection scheme that is active below a specific speed w_0 was used for the current injection. The averaging scheme was implemented as a function of speed. The appropriate sample size for different speed ranges were determined and tabulated. The noise in the measurements at low speed is removed by the averaging and is therefore helpful in getting a more accurate back-EMF estimation.

7

Testing of Algorithm

This chapter describes the testing of the algorithm to different speeds inputs at various current injections. It studies the robustness of the solutions at various conditions and its suitability for different application. Section 7.1 describes how the algorithm's performance was analyzed. Section 7.2 and Section 7.3 describe the stability and power issues of the control scheme respectively. Finally, Section 7.4 gives the conclusions from the test results.

7.1 Algorithm testing

The first step involves testing the implementation of the sensorless algorithm without any improvement schemes added to it. The current software was calibrated and modified to work on the LPC1800 and for the chosen motor. At each stage the program was run in debug mode to check the values of variables in the program. Once the angle estimation was reached, the graphical user interface was used to test if the angle estimated was equal or within the error limit.

7.1.1 Angle Estimation testing

The sensorless algorithm's accuracy and overall stability can be studied by how close the estimated angle is to the actual angle measured using the quadrature sensors. The comparison between the estimated and actual angle is done using the motor control GUI's scope tool. The quadrature encoder value is in the range 0 to .99 which corresponds to the angle 0 to 360 degrees.

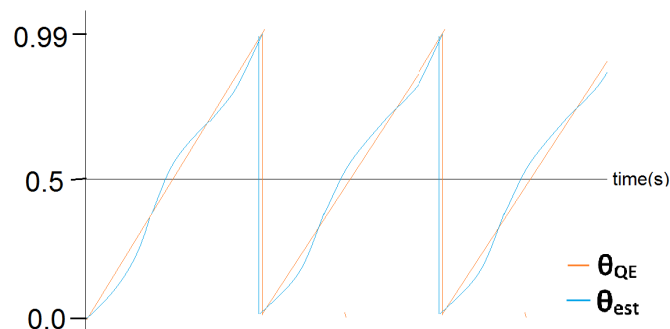


Figure 7.1: Scope result from GUI comparing the estimated and sensed angle

From the Figure 7.1 it can be observed that the estimated and the encoder reading

is slightly out of phase. The filters used in the model creates a phase lag and makes the estimated angle out of phase with the actual angle. This error is tabulated for different speeds and compensated by adding an offset in the estimated angle.

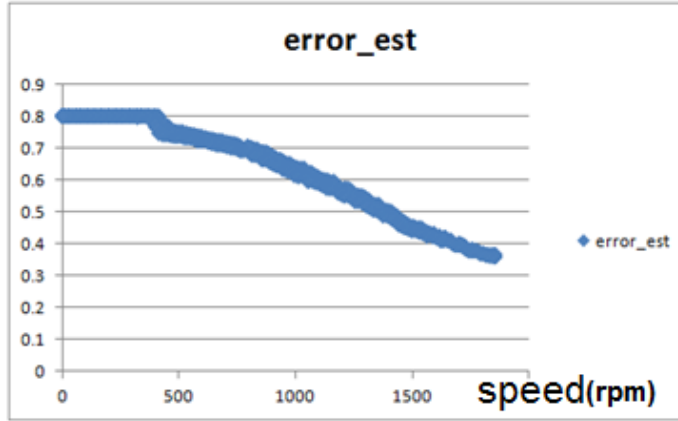


Figure 7.2: Angle compensation as a function of speed

Figure 7.2 shows the angle compensation as a function of speed. From Fig. 7.1 the error in the estimated angle is found to have three maximums in one rotation. The possible reason for this is the error due on the alignment of rotor along the three supply phases. The angle compensation scheme implemented in this thesis is only a function of speed and hence it is two dimensional as shown in Fig. 7.2. However, if the error caused due to positional variation needs to be compensated, then a second variable needs to be added to the compensation function. This variable is be the uncompensated angle itself. Thus, the final compensation scheme will have a lookup table that is three dimensional. This thesis presents only the two dimensional method of compensation to simplify the scheme.

To measure the improvements on the algorithm due to the improvement schemes, first the error limit of the speed estimation was defined as ± 80 rpm. Further at low speed the error limit was set as 15% of the set motor speed. Four different cases are studied to compare the effects of each improvement scheme. These cases are as follows.

1. Sensorless without any improvement added
2. Sensorless with current injection alone
3. Sensorless with averaging
4. Sensorless with both the improvements

The error in the estimated and the actual speed for four different cases is shown in the figures below.

Case 1: Sensorless algorithm without any improvements.

The sensorless solution without any suggested improvements was tested on the motor for quantifying the speed limits. The response of the motor to the sensorless is given in

the Fig. 7.3. The speed error is plotted against the set speed in Fig. 7.4.

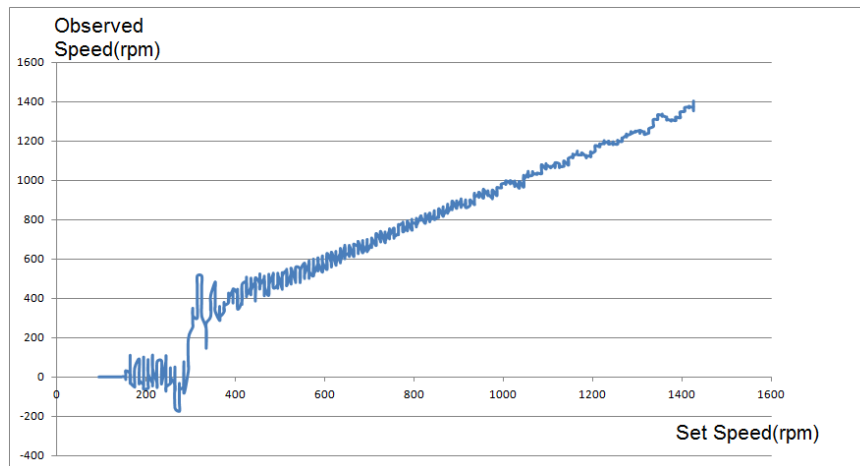


Figure 7.3: The actual rotor speed vs set rotor speed(case 1)

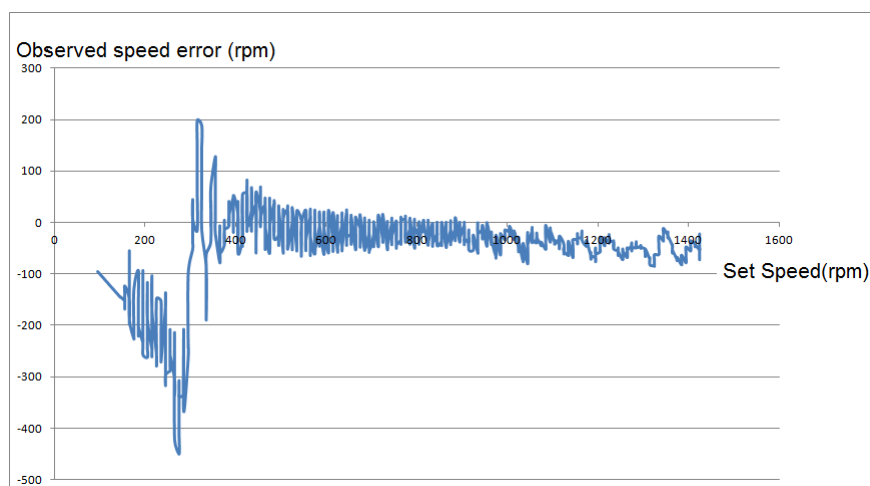


Figure 7.4: The speed error plotted against the set speed(case 1)

It can be seen from Fig.7.3 that the performance of the control is not good for speeds below 450rpm(error greater than 80rpm). The proposed improvements were made in the algorithm through the software changes and were run again at the same speed range with all remaining parameters constant.

Case 2: Sensorless with current injection.

The effect of adding current injection to the sensorless scheme is shown in Figure 7.5 and 7.6. At low speed, the effect of current injection can be seen in the figure 7.5. As

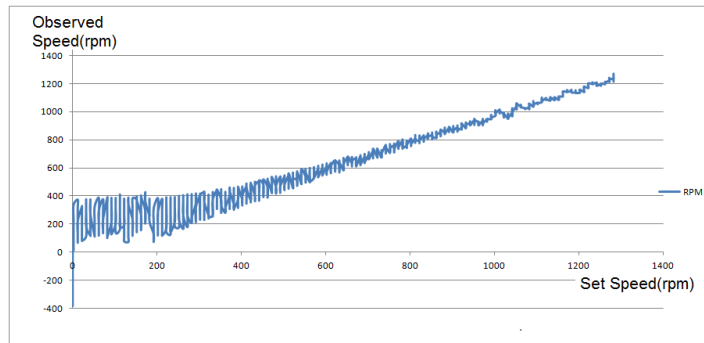


Figure 7.5: The actual rotor speed vs set rotor speed(case 2)

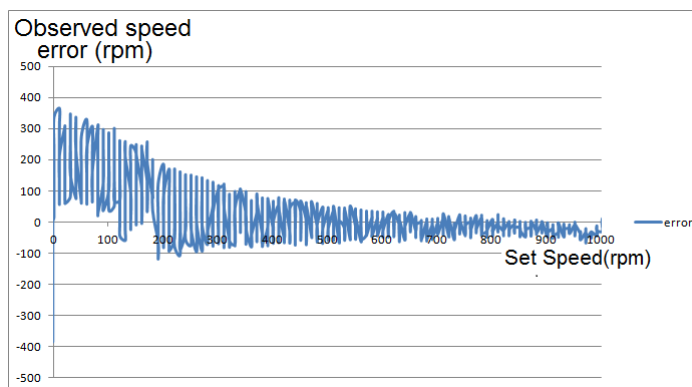


Figure 7.6: The speed error plotted against the set speed(case 2)

expected, the presence of back-EMF signal is making it possible to control the motor at low speed. However, the error analysis in Fig. 7.6 shows that below the speed of 400rpm the error limit exceeds the allowable limit (80rpm). The cause of error is due to the noise and the accumulation of angle estimation error over the numerous PID loops. At low speed, the loops per rotation is large compared to higher speed. Thus, in the absence of accurate angle estimation this error will persist.

Case 3: Sensorless scheme with averaging method added.

To analyze the effect of averaging the sensorless scheme was tested in the presence of current averaging without the application of current injection. The figure 7.7 and 7.8 shows the results of this test.

As expected, the averaging scheme has very little effect on determining the lower limit of speed control. Thus, this method is not useful if used without any other additional schemes. The purpose of averaging is to filter out the noise and give a measurable value of back-EMF. From the figures 7.7 and 7.8, it can be seen that the averaging scheme gives a measurable speed even below 200rpm. This aspect could be beneficial when used along with the current injection scheme. The speed response in Fig. 7.7 is much smoother compared to the speed response in Fig. 7.3. Thus,

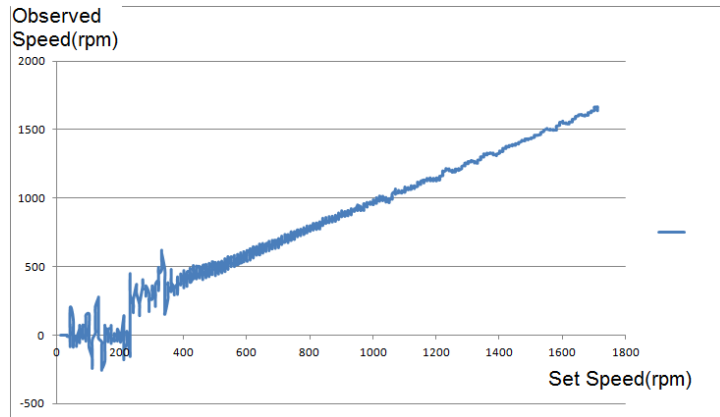


Figure 7.7: The actual rotor speed vs set rotor speed(case 3)

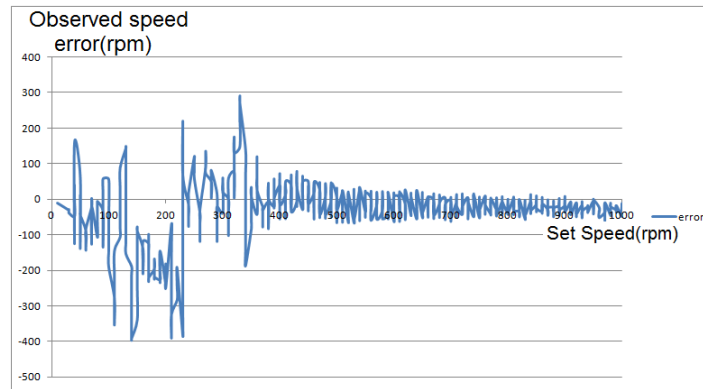


Figure 7.8: The speed error plotted against the set speed(case 3)

averaging scheme acts as a low pass filter and helps in achieving a smoother speed control.

Case 4: Sensorless with both the improvements.

The results of tests on case 4 are shown in Fig. 7.9 and 7.10. When both the improvements were applied, the lowest stable speed obtained was 50rpm. However, the control had instabilities in the range 220rpm to 440rpm (Fig. 7.10). The instabilities in the speed control were suspected to be due to the PID alone. To check if PID was the cause of the instabilities, the PID loops were disabled and the sensorless solutions were tested for the current injection and averaging methods. This resulted in same test result for case 4. Hence, it was concluded that PID was not the cause for the instabilities. The angle estimation was directly checked for the speed range 220rpm to 400rpm. The estimated angle was found to deviate from actual angle by large values in this range. Hence, the cause for the instability is the incorrect angle estimation for the range 220rpm-440rpm.

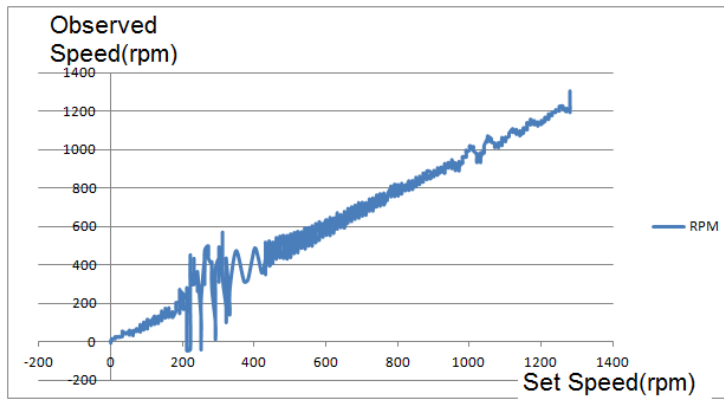


Figure 7.9: The actual rotor speed vs set rotor speed(case 4)

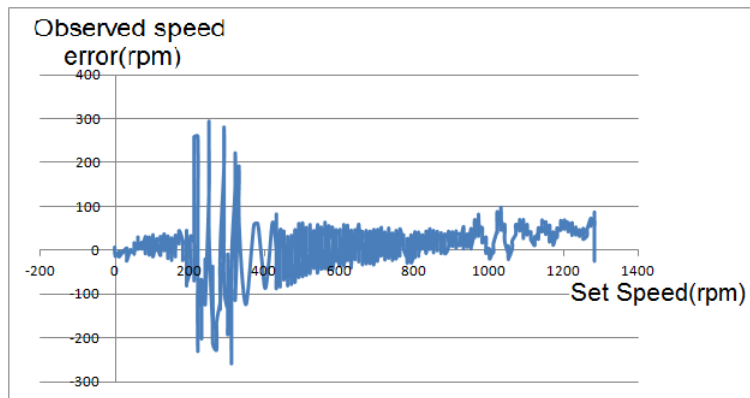


Figure 7.10: The speed error plotted against the set speed(case 4)

7.2 Motor Control stability

The motor speed response was compared with the 15% set speed value to check the range of speed for which the error is within allowable range. From Figure 7.11, the region of stability can be identified as the region in which the error signal (green) is within the V shape of the 15% set speed lines (red and blue). This region is identified as between 220rpm and 440rpm. From Table 7.1, the effect of current injection and averaging is not impressive with a maximum error of 270rpm and maximum % error of 100 within its full range of operation. However, if one excludes the unstable range from 200rpm to 400rpm, the control performance is better. In its stable range the maximum error is 80rpm and the maximum percentage error is 15%.

7.3 Power efficiency

The motor algorithm needs to be tested for its power efficiency at low speeds. The current drawn from the supply before starting the motor is .11A. This current is used

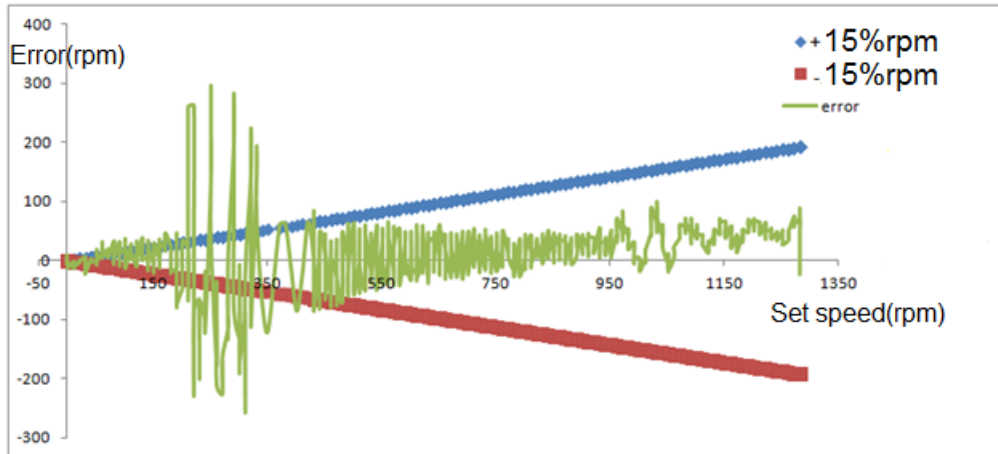


Figure 7.11: The speed error, +/- 15% of set speed plotted against the set speed

Table 7.1: Comparison of control performance achieved in different cases

Cases	Sensorless	Current injection	Averaging	Current Inj. & Avg.
lowest RPM	450	450	450	50
Maximum error(RPM)	440	350	400	270
Maximum % error(RPM)	180	250	270	100

in the controller board. When the motor is running, the current drawn from the power source increases. The maximum current drawn from the supply at low speed range is 1.5A. Therefore, 1.39A is drawn by the motor at 22V input voltage. Thus 33W of power is used in motor control at low speed. This is leading to problems of power dissipation. There are two causes of this high current at the low speed range. First the current injected into the d-axis is not completely isolated from the q-axis. Therefore, indirectly there is current injection into the q-axis as well. Secondly, the angle estimation error is significant at low speed. If the supplied voltage and the current is not in phase, then there is loss of power in the control system. Thus, after a few minutes (5 minutes) of rotating the motor at speeds less than 200rpm, the motor gets overheated.

7.4 Conclusions

The process of testing and implementation of algorithm has shown some advantages and disadvantages of the proposed improvement schemes. They are summarized here.

Advantages

1. The sensorless scheme is now able to work at speeds as low as 50rpm with less than 15% error.

2. Both the schemes can be applied to the existing solution without any hardware modification.
3. The control scheme does not depend on the saliency of the motor.

Disadvantages

1. The current averaging scheme affects the efficiency of the motor adversely.
2. The motor parameters are required for calibrating the schemes.
3. The angle estimation in the current form is not accurate enough at low speed.

Conclusion and Future Work

The purpose of the thesis was to develop and implement a sensorless algorithm for low speed and test it on a PMSM motor. In this chapter the conclusions drawn from the various tests on the motor using the algorithm with different compensation schemes are given. Section 8.1 gives the conclusion of the thesis work. In section 8.2 the future improvements to the solution is proposed.

8.1 Conclusions

The objective of low speed control of PMSM was achieved in the thesis. PMSM was controlled at low speed range of 50rpm to 220rpm. The conclusions from the thesis can be summarized as given below.

1. The two proposed schemes: current injection and current averaging were implemented on a rotating frame of FOC based sensorless solution. The current injection was carried out in the d-axis of the rotating frame. For speed less than 800rpm the current injection was applied. The current averaging with dynamic sampling rate was done to further improve the low speed control. Both the schemes were implemented in NXP microcontroller.
2. The lowest speed control achieved for the new scheme is between 45-50rpm. This is a significant improvement from the previous sensorless solution which had a lower limit of 400-450rpm.
3. The stability and power issues of the new control were also studied. The d-axis and q axis current loops were found to be coupled at low speeds. This means whenever current is injected to d-axis, q-axis also draws current. At low speed this leads to significant current(.5A-1.5A) being drawn from the power source. This leads to power wastage in the form of motor heat dissipation.
4. The angle error compensation was achieved using two dimensional compensation. However this scheme still produces errors because angle offset was found to be a function of rotor position. The error in angle estimation affects the speed estimation directly. Hence, there is an instability in the speed control for speeds between 220rpm and 450rpm.

8.2 Possible improvements in the future

A better feedback topology which compensates the effect of coupling between the two axes (d-q) will lead to a more stable and power efficient low speed control solution. It

was assumed in the thesis that current injected into the d-axis will not affect the q-axis current due to the separate feedback loops for the two currents. However during the testing, the current in the q-axis was found to be coupled with d-axis currents. Therefore, improvements in the decoupling scheme will lead to better performance of the algorithm. As explained in Section 7.1 this thesis uses a two dimensional angle compensation method to offset the error in angle estimation. The angle estimation can be improved if a three dimensional position based compensation scheme is used instead of speed based compensation. Hence, the topics that can be explored for improvements of this scheme are given below.

- Decoupling control of d and q axis currents.
- Improved feedback topology for PID loops.
- Position based angle correction (3-dimensional angle correction).

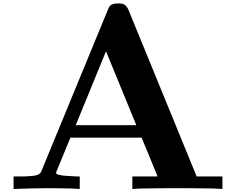
Bibliography

- [1] Atmel, *Avr447: Sinusoidal driving of three phase permanent magnet motor using atmega48/88/168*, <http://www.atmel.com/Images/doc8010.pdf>, Accessed July, 2012.
- [2] R.; Zerdali E.; Inan-R. Barut, M.; Demir, *Real-time implementation of bi input-extended kalman filter-based estimator for speed-sensorless control of induction motors*, IEEE Transactions on Industrial Electronics **59** (2012), no. 11, 4197–4206.
- [3] A. Consoli, G. Scarcella, and A. Testa, *Sensorless control of ac motors at zero speed*, Industrial Electronics, 1999. ISIE '99. Proceedings of the IEEE International Symposium on **1** (1999), 373–379.
- [4] M. J. Corley and R. D. Lorenz, *Rotor position and velocity estimation for a salient-pole permanent magnet synchronous machine at standstill and high speeds*, IEEE Trans. Ind. Applicat. **34** (1995), 240–247.
- [5] Drivetechnic Dal Y. Ohm, *Dynamic model of pm synchronous motor*, http://www.drivetechnic.com/articles/IM97PM_Rev1forPDF.pdf, Accessed July, 2012.
- [6] Xu Wenli; Ling Qiang; Chen Feng, *High precision observer of an induction motor with variable structure control*, Intelligent Control and Automation, 2000. Proceedings of the 3rd World Congress on **4** (2000), 2996.
- [7] J.W.. Finch, *Scalar and vector: a simplified treatment of induction motor control performance*, Vector Control Revisited , IEE Colloquium on (1998), 2.
- [8] Freescale, *Sensorless pmsm control for an h-axis washing machine drive*, http://cache.freescale.com/files/microcontrollers/doc/ref_manual/DRM110.pdf, Accessed July, 2012.
- [9] Kenichi Iizuka, Hideo Uzuhashi, Minoru Kano, Tsunehiro Endo, and Katsuo Mohri, *Microcomputer control for sensorless brushless motor*, Industry Applications, IEEE Transactions on **21** (1985), no. 3, 595–601.
- [10] D. Janiszewski, *Extended kalman filter based speed sensorless pmsm control with load reconstruction*, IEEE Industrial Electronics, IECON 2006 - 32nd Annual Conference on (2006), 1465–1468, 6–10.
- [11] P.L. Jansen and R.D. Lorenz, *Transducerless position and velocity estimation in induction and salient ac machines*, Industry Applications, IEEE Transactions on **31** (1995), no. 2, 240–247.
- [12] W. Kaewjinda and M. Konghirun, *Vector control drive of pmsm using resolver sensor*, ECTI transaction on Electrical Engineering, Electronics and communications **5** (2007), no. 1.

- [13] Yung kang Chin, *A permanent magnet synchronous motor for an electric vehicle-design analysis*, Electrical Machines And Power Electronics Department Of Electrical Engineering Royal Institute Of Technology Sweden (2004), Ph.D Thesis.
- [14] Hongrae Kim, M. Amirabadi, S. Englebretson, and W.M. Arshad, *Current observer based position estimation using the stationary frame equivalent of a synchronous frame pi regulator for pmsm sensorless drives*, Electric Machines and Drives Conference (IEMDC) IEEE International (2011), 581–586.
- [15] K. H. Kim, *An improved stationary frame based current control scheme for a permanent magnet synchronous motor*, IEEE Transactions on Industrial Electronics **50** (2003), no. 5, 1065–1068.
- [16] Yong-Kil Lee Tae-Hyun Won Han-Woong Park Yong-Il Jung Man Hyung Lee Lee H. Kim Mun-Soo, Dall-Sup Song, *A robust control of permanent magnet synchronous motor using load torque estimation*, Industrial Electronics Proceedings. ISIE IEEE International Symposium on **2** (2001), 1157.
- [17] AO Smith Lonel, D. M., *Brushless interior permanent magnet(ipm) motors- a new solution for high performance appliance*, <http://www.aosmith.com/>, Accessed July, 2012.
- [18] M.R.; Milimonfared J. Malekian, K.; Sharif, *An optimal current vector control for synchronous reluctance motors incorporating field weakening*, 10th IEEE International Workshop on Advanced Motion Control, AMC (2008), 393.
- [19] S. Moromito, *Sensorless control strategy for salient pole pmsm based on extended emf in rotating reference frame*, IEEE Transactions on Industrial Applications **38** (2002), no. 4, 1054–1061.
- [20] Maxon Motor, *Maxon ec motor*, <http://www.maxonmotor.com/maxon/view/catalog/>, Accessed July, 2012.
- [21] Aixian Pan and Hongcai Zhao, *Direct control of the stator flux linkage applying in the permanent magnet synchronous motor*, ICMA, International Conference on Mechatronics and Automation (2009), 3668.
- [22] J. Persson, M. Markovic, and Y. Perriard, *A new standstill position detection technique for nonsalient permanent-magnet synchronous motors using the magnetic anisotropy method*, Magnetics, IEEE Transactions on **43** (2007), no. 2, 554.
- [23] Texas Instruments Platnic, M., *Implementation of vector control for pmsm using the tms320f240 dsp, dec 2008*, <http://www.ti.com/lit/an/spra494/spra494.pdf>, Accessed July, 2012.
- [24] Allan B. Plunkett and Fred G Turnbull, *Load-commutated inverter/synchronous motor drive without a shaft position sensor*, Industry Applications, IEEE Transactions on **15** (1979), no. 1, 63–71.

- [25] M. Schrodli and M. Lambeck, *Statistic properties of the inform method for highly dynamic sensorless control of pm motors down to standstill*, Industrial Electronics Society, 2003. IECON '03. The 29th Annual Conference of the IEEE **2** (2003), 1479–1486.
- [26] Steven W. Smith, *The scientist and engineer's guide to digital signal processing*, California technical publishing, 1997.
- [27] Hrabovcova V. Stulrajter, M. and M. Franco, *Permanent magnet synchronous motor control theory*, Journal of Electrical Engineers **58** (2007), no. 2, 79.
- [28] Evgen Urlep and Karel. Jezernik, *Low and zero speed sensorless control of nonsalient pmsm*, Industrial Electronics, 2007. ISIE 2007. IEEE International Symposium on (2007), 2238.
- [29] A. Veltman, P.P.J. van den Bosch, and R.J.A. Gorter, *Fish method based state estimation for controlling inverter driven machines*, Power Electronics Specialists Conference, PESC '94 Record., 25th Annual IEEE , **1** (1994), no. 2, 758–762.
- [30] D.W.J.; Doncker R.W.De Veltman, A.; Pulle, *Fundamentals of electrical drives*, Springer, 2007.
- [31] Microship Technology Inc Zambada, J., *Sensorless field oriented control of pmsm motors*, <http://ww1.microchip.com/downloads/en/AppNotes/01078A.pdf>, Accessed July, 2012.
- [32] A. Zentai and T. Daboczi, *Improving inform calculation method on permanent magnet synchronous machines*, Instrumentation and Measurement Technology Conference Proceedings, 2007. IMTC 2007. IEEE (2007), 1–6,1–3.
- [33] Zedong Zheng, Yongdong Li, and M. Fadel, *Sensorless control of pmsm based on extended kalman filter*, Power Electronics and Applications, 2007 European Conference on (2007), 1–8,2–5.

Appendix



A.1 The observer block flow diagram

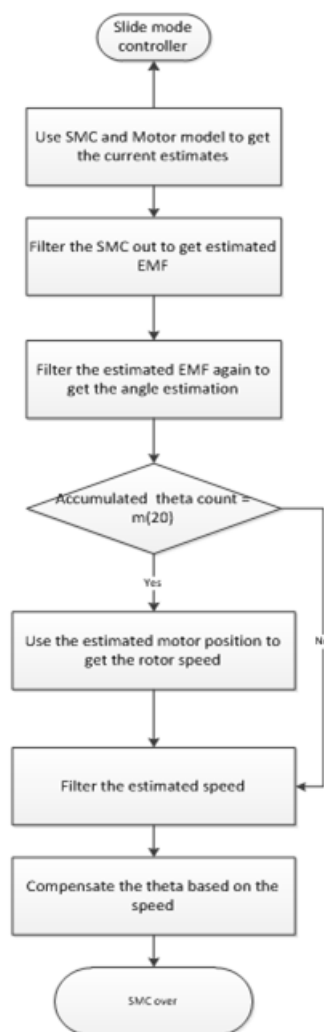


Figure A.1: Flow digram of the observer block

A.2 The Testbench setup

. The figure shows the testbench setup which was used for testing and debugging the algorithm.

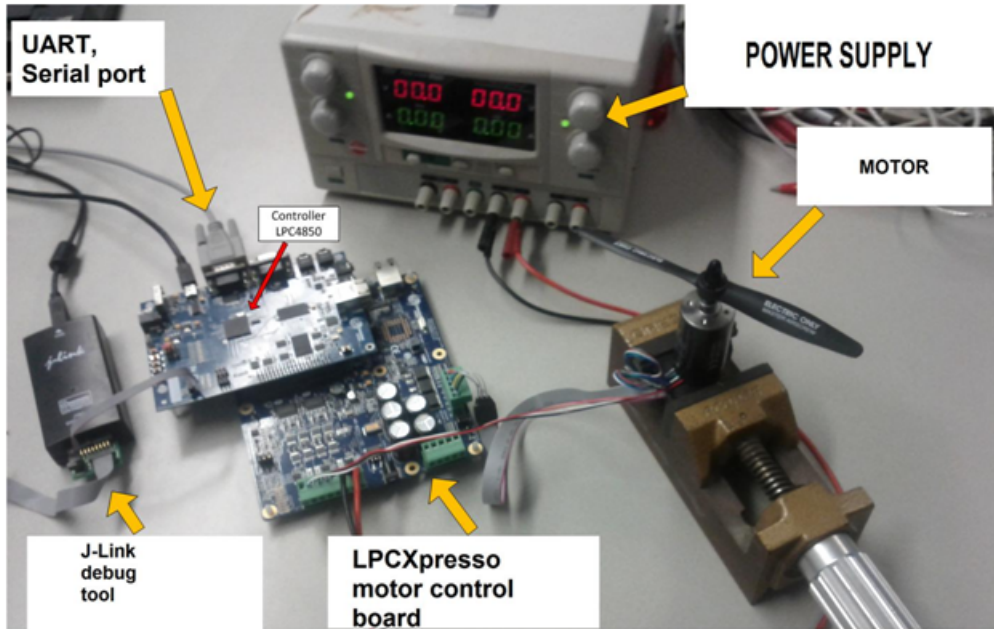


Figure A.2: Experimental setup